A Systematic Interrogation of MHC Class I Antigen Presentation Identifies Constitutive and Compensatory Protein Degradation Pathways

Jennifer L. Mamrosh[1,2], Jing Li[1,2], David J. Sherman[1,2], Annie Moradian[3], Michael J. Sweredoski[3], Rati Verma[1,2], James A. Johnston[2], J. Russell Lipford[2], Raymond J. Deshaies[1,2*]

1. Division of Biology and Biological Engineering, California Institute of Technology, Pasadena, CA 91125, USA.
2. Amgen Research, Thousand Oaks, CA 91320, USA.
3. Proteome Exploration Laboratory, California Institute of Technology, Pasadena, CA 91125, USA.

*Corresponding author: Raymond J. Deshaies, rdii2003@gmail.com

ABSTRACT

Protein degradation products are constitutively presented as peptide antigens by MHC Class I. While hypervariability of Class I genes is known to tremendously impact antigen presentation, whether differential function of protein degradation pathways (comprising >1000 genes) could alter antigen generation remains poorly understood apart from a few model substrates. In this study, we introduce normalization methods for quantitative antigen mass spectrometry and confirm that most Class I antigens are dependent on ubiquitination and proteasomal degradation. Remarkably, many antigens derived from mitochondrial inner membrane proteins are not. Additionally, we find that atypical antigens can arise from compensatory protein degradation pathways, such as an increase in mitochondrial and membrane protein antigen presentation upon proteasome inhibition. Notably, incomplete inhibition of protein degradation pathways may have clinical utility in cancer immunotherapy, as evidenced by appearance of novel antigens upon partial proteasome inhibition.

INTRODUCTION

To survive, organisms must be able to detect threats in their environment. While all multicellular organisms have an innate immune system broadly surveying for common pathogen characteristics, evolution of an adaptive immune system in jawed vertebrates allowed for specific and lasting responses to wider threats. Central to adaptive immunity is the display of antigens. All nucleated cells express on their cell surface peptide antigens derived from intracellular proteins. This represents the current state of cells to the immune system and allows for the detection of intracellular infection by bacteria and viruses. Peptide antigens typically of nine amino acids in length generated from intracellular proteins are presented in a non-covalent complex with the plasma membrane protein MHC Class I. These antigens, originating as longer peptides generated by proteasomal degradation, often are subject to additional trimming by proteases in the cytoplasm and endoplasmic reticulum before being loaded onto MHC Class I *(reviewed in Rock et al., 2016).*

Which antigens are displayed by MHC Class I is dependent on binding preferences of hypervariable Class I genes (*HLA-A,-B,-C*) *(Lundegaard et al., 2010).* Far less is understood regarding how antigens are generated from intracellular proteins by protein degradation pathways. Although it is apparent that proteasomal degradation of proteins tagged for destruction by ubiquitination is required for the bulk of antigen generation *(Michalek et al., 1993; Rock et al., 1994; Wei et al., 2017),* whether specific genes in these pathways *(reviewed in Saeki, 2017)* play an outsized role remains unknown.

Here, we present a systematic survey of the role of protein degradation pathways in MHC Class I antigen presentation. Technical optimizations were made to enable high-throughput and quantitative antigen mass spectrometry following chemical inhibition of protein degradation pathways, allowing us to define particular antigens amongst the thousands identified dependent on these pathways. Most experiments were performed in immortalized B lymphoblasts, which abundantly present MHC Class I antigens while generally not cross-presenting antigens typically associated with MHC Class II derived from extracellular or endolyosomal pathway proteins *(Ke et al., 1996)*. Initially, we inhibited ubiquitination and proteasomal degradation, and observed that, as expected, these pathways are largely required for antigen presentation. However, we also identified evidence for compensatory pathways that presented atypical antigens when these canonical pathways were inhibited, as well as a surprising number of proteasome-dependent substrates less dependent on ubiquitination. This prompted us to consider the relative contributions of autophagy as well as proteasome-associated factors such p97/VCP to antigen generation. Our experiments demonstrate that these protein degradation pathways generate specific

types of antigens, and also suggest that antigen display is relatively robust in the face of environmental insult to protein degradation pathways. Remarkably, partial inhibition of the proteasome also induces the presentation of a small number of atypical antigens. We suggest that these may be novel therapeutic targets in a cancer immunotherapy setting.

RESULTS

MHC Class I antigen mass spectrometry is improved by methodology for more accurate data normalization and removal of 'background antigens'.

We purified MHC Class I antigens as previously described *(Chong et al., 2018)*, and subsequently labeled samples on their N-termini to enable multiplexing in a single mass spectrometry run. Additionally, we mixed a "spike-in standard" consisting of mouse MHC Class I presenting a defined antigen (SIINFEKL) at a 1:100 ratio based on cell number with our human cell lysates. This mouse MHC Class I/SIINFEKL standard was then co-purified with human MHC Class I complexes **(Figure 1A).** The spike-in standard enables more accurate normalization to correct for potential sample loss during the antigen purification steps. Additionally, it allows for normalization when experimental treatment alters overall antigen presentation. To demonstrate this, B lymphoblasts were treated with the secretion inhibitor brefeldin A for 16h, which inhibits transport of MHC Class I to the cell surface *(Cox et al., 1990).* This did not alter viability **(Supplemental Figure 1A)**, and antigens quantified by mass spectrometry were as expected in size, being primarily 9mer peptides **(Supplemental Figure 1B)**. Whereas brefeldin A reduced overall MHC Class I antigen presentation as evidenced by total peptide intensity measured by mass spectrometry, levels of the spike-in standard were not affected **(Figure 1B)**. Statistical analysis of mass spectrometry data by widely used data normalization methods like total intensity normalization, however, obscure this treatment-induced decrease in total antigen presentation **(Figure 1C)**. Normalization to the spike-in standard avoids this artifact, while also correcting for any potential sample loss during processing steps.

Ultimately, we aimed to perform experiments on cells treated with protein degradation pathway inhibitors for much shorter periods of time due to the toxicity of inhibiting core pathways. Removal of pre-existing MHC Class I complexes by brief incubation of cells in mild acid solution ("acid stripping") *(Sugawara et al., 1987; Montealegre et al., 2015)* resulted in > 90% reduction in cell surface Class I complexes, with substantial recovery by 4h **(Supplemental Figure 1C)**. Cells were pre-treated for 2h with either brefeldin A, the translation inhibitor cycloheximide to block new MHC Class I production, or vehicle, and then acid stripped. Cells were immediately collected following acid stripping, or else cultured again for 4h with inhibitors **(Figure 1D).** We observed that total peptide antigen intensity measured by mass spectrometry was markedly reduced following acid stripping or cycloheximide treatment; this reduction was consistently lesser with brefeldin A despite varying in magnitude between the two cell lines **(Figure 1E),** suggesting loaded MHC Class I complexes can potentially be purified from the ER even if not transported to the cell surface. Nevertheless, total antigen abundance was not as reduced as we expected even following acid stripping or cycloheximide treatment. We considered that this might be a limitation of mass spectrometry, such as background quantification. Additionally, the preference of mass spectrometry for quantifying abundant peptides *(Schmidt et al., 2008)* likely biases towards selection of antigens decreasing less in response to treatment. To better understand these 'background antigens', we specifically considered the effects of cycloheximide treatment, which was comparable to effects seen immediately upon acid stripping **(Supplemental Figure 1D)**. We observed that antigens that did not significantly decrease in response to cycloheximide were lower in intensity, leading us to suspect that many antigens near the limit of detection by mass spectrometry suffer from

background quantification or are too variable to detect a significant decrease **(Figure 1F)**. For most subsequent mass spectrometry experiments, we included 2 cycloheximide-treated replicates, and excluded from further analysis antigens not decreasing greater than 1.5 fold in response to cycloheximide in both replicates. This filter removed from further consideration a large number of "background antigens" that were not statistically significant **(Figure 1G)**, without requiring the three or more replicates needed for a cutoff based on statistical significance. We then sought to apply this optimized methodology for quantitative antigen mass spectrometry to determining the role of diverse protein degradation pathways in MHC Class I antigen generation **(Figure 1H)**.

Inhibition of ubiquitination and proteasomal degradation results in a net decrease in antigen presentation, yet paradoxical increases in certain antigens

In four B lymphoblast cell lines with largely distinct MHC class I alleles **(Supplemental Figure 1E)**, we planned to inhibit ubiquitination with the ubiquitin activating enzyme E1 inhibitor MLN7243 and the proteasome with carfilzomib. We determined a dose of MLN7243 (500 nM) resulting in disappearance of most polyubiquitinated proteins with 4h of pretreatment **(Supplemental Figure 2A)**, and a dose of carfilzomib (1 μM) resulting in near complete proteasome inhibition with 1h of pretreatment **(Supplemental Figure 2B)**. For mass spectrometry experiments, cells were pretreated with these inhibitors, pre-existing antigens removed by acid stripping, and cells treated again with inhibitors for 4h. These treatments did not impact cell viability **(Supplemental Figure 2C)**. As measured by flow cytometry **(Supplemental Figure 2D)** and mass spectrometry **(Supplemental Figure 2E)**, inhibition of ubiquitination or proteasomal degradation reduced overall antigen presentation.

Reduction in antigen presentation upon inhibition of ubiquitination or proteasomal degradation was unlikely to be a nonspecific outcome of inhibitor toxicity, as we performed mass spectrometry on cells treated with similarly toxic or more toxic doses of the DNA damaging agent cisplatin **(Supplemental Figure 2F)**, and observed significant decreases in antigen presentation only at levels of cisplatin treatment substantially more toxic than that of proteasome inhibition **(Supplemental Figure 2G)**. Whereas we observed an expected decrease in antigen presentation upon inhibition of ubiquitination or proteasomal degradation, a substantial fraction of antigens was not significantly decreased by these treatments **(Supplemental Figure 2H)**. Some of these antigens showed a trend towards decreasing that might become statistically significant if larger sample sizes were used. Nevertheless, we considered the possibility that antigens presented seemingly independent of the ubiquitin-proteasome system could be produced by alternative pathways. We determined the subcellular localization of antigen source proteins for antigens significantly decreased by both carfilzomib and MLN7243 treatment ("UPS-dependent"), and those not significantly decreased by either treatment ("UPS-independent") **(Figure 2A).** Antigens not significantly decreasing were more likely to be derived from mitochondrial inner membrane proteins **(Figure 2B)**, a region of the cell inaccessible to proteasomes. Additionally, antigens not significantly decreased by MLN7243 or carfilzomib treatment were more likely to be longer in length than the typical 9mer **(Figure 2C)**, suggesting that protein fragments produced by the proteasome are more optimal for MHC Class I antigen display.

In addition to antigens significantly decreased by MLN7243 and carfilzomib treatment, and those not significantly changing**,** we were surprised to also observe antigens paradoxically increasing in response to these treatments **(Supplemental Figure 2H, I)**. Significantly increased antigens often appear inhibitor specific **(Figure 2D)**, suggesting they are not produced by nonspecific cell stress pathways; in support of this, we also observed few increased antigens by cisplatin treatment beyond rapidly induced proteins like HMOX1 *(McMahon et al., 2018)* **(Supplemental Figure 2G).** By comparing significantly increased versus significantly decreased antigens across all cell lines, we observed that antigens significantly

decreased in response to proteasome inhibition were more likely to come from cytosolic and nuclear proteins, whereas those that increased were more likely to be from single pass membrane proteins, particularly type 1 membrane proteins, and mitochondrial inner membrane proteins **(Figure 2E).** Antigens increased by inhibition of ubiquitination were also more likely to come from mitochondrial inner membrane proteins. Therefore, we suspected that antigens increased by proteasome inhibition, and perhaps inhibition of ubiquitination, were from proteins typically not exposed to the proteasome (e.g. mitochondrial and membrane proteins) and instead were degraded by proteases, perhaps in the lysosome through compensatory autophagy.

To test the hypothesis that antigens increased by proteasome inhibition were produced by autophagy or other forms of lysosomal degradation, we treated cells with carfilzomib in the presence or absence of the autophagy/lysosomal inhibitor leupeptin **(Supplemental Figure 2J)**, and quantified antigen presentation by mass spectrometry. Leupeptin treatment decreased overall antigen presentation, although less so than carfilzomib **(Supplemental Figure 2K)**, potentially due to its milder inhibition of select proteasomal activity *(Kisselev et a., 2006).* Similarly, we also treated cells with carfilzomib in the presence or absence of an ATG7 inhibitor *(Huang et al., 2020)* **(Supplemental Figure 2L)**, which decreased antigen presentation less significantly than leupeptin **(Supplemental Figure 2M)**. The overall effect of carfilzomib on antigen presentation did not differ significantly from that of carfilzomib plus leupeptin or the ATG7 inhibitor **(Supplemental Figure 2N, O)**; these autophagy inhibitors also did not prevent the increased presentation of certain antigens observed with carfilzomib treatment **(Figure 2F)**. Therefore, autophagy or lysosomal degradation, at least that able to be inhibited by the lysosomal enzyme inhibitor leupeptin or the ATG7 inhibitor blocking the induction of autophagy, does not appear to be the major source of antigens increased by carfilzomib treatment.

We appreciated that atypical antigens may still be able to be loaded onto free or recycled MHC Class I in the endolysosomal system, even if not produced by autophagy. Peptide loading or exchange could also occur at the cell surface. Atypical antigen presentation pathways such as these may only become apparent in the absence of a larger supply of canonical antigens produced by the proteasome. To test this hypothesis, we treated a B lymphoblast cell line homozygous for HLA-A and HLA-B alleles with purified peptides identified previously by antigen mass spectrometry able to bind these alleles (TIAPALVSK and YPTTTISYL for HLA-A*03:01 and HLA-B*35:03, respectively). Cells were also treated with carfilzomib, alone or in combination with these competition peptides. The competition peptides were loaded onto MHC Class I, being amongst the most abundant antigens detected by mass spectrometry. The competition peptides were also relatively abundant when compared with antigens significantly increased by carfilzomib treatment **(Supplemental Figure 2P)**. The competition peptides also had predicted affinities for HLA-A and HLA-B higher than the majority of antigens, including the groups of all antigens identified by mass spectrometry and antigens significantly increased by carfilzomib treatment **(Supplemental Figure 2Q)**. Therefore, we expect the competition peptides are sufficiently abundant and of high enough affinity to outcompete most antigens increased by carfilzomib if these antigens were loaded in the endolysosomal system or at the cell surface. As expected, treatment with the competition peptides did not substantially alter overall antigen presentation, suggesting they do not affect the presentation of canonical antigens produced by the proteasome and loaded in the endoplasmic reticulum **(Supplemental Figure 2R)**. Increased antigen presentation by carfilzomib was only significantly reduced in one instance by the competition peptides **(Figure 2G)**, leading us to conclude that antigens induced by proteasome inhibition are also likely to be loaded in a conventional manner.

Therefore, we considered additional sources for the production of antigens increased by inhibition of ubiquitination or proteasomal degradation. Bioinformatic searches identified mitochondrial

metalloprotease YME1L1 as being enriched in being a binding partner of source proteins for the peptide antigens that were increased by proteasome inhibition. **(Figure 2H).** Cleavage by YME1L1 would allow for antigen sampling from mitochondrial inner membrane proteins that are protected from proteasomes. We also found that source proteins for antigens increased by inhibition of ubiquitination were more likely to be reported binders of ubiquitin-binding proteins HRS and GGA1 involved in protein sorting in the trans-Golgi network *(Raiborg et al., 2002; Wang et al., 2007)* **(Figure 2H).** It is possible some atypical sorting pathway directs these proteins producing antigens increased by MLN7243 to lysosomal (or other nonproteasomal) degradation. It is also possible that proteases in other cellular compartments (e.g. cytosolic, nuclear, endoplasmic reticulum) contribute to protein degradation and antigen generation in the absence of the ubiquitin proteasome system.

Antigens only partially dependent on the ubiquitin-proteasome system share unifying characteristics

Given the differences in localization for antigens increased by inhibition of ubiquitination versus proteasomal degradation, we aimed to further define groups of antigens only partially dependent on the ubiquitin-proteasome system for their generation. We identified antigens that differed significantly in their response to MLN7243 or carfilzomib treatment in all cell lines, and grouped these antigens into "quadrants" **(Figure 3A; Supplemental Figure 3A,B).** These groupings can be generally understood as antigens particularly increased by proteasome inhibition (QI) or ubiquitination inhibition (QII), and antigens less ubiquitin-dependent (QIII) and those less proteasome-dependent (QIV). In support of these classifications, reported ubiquitin-independent proteasome substrate ODC1 *(Murakami et al., 1992)* was observed in the expected QIII **(Figure 3A).** We then assessed whether subcellular localization and molecular function of antigen source proteins in these 4 quadrants were significantly different from antigens significantly decreased by both MLN7243 and carfilzomib. We observed that antigens in QI were more likely to come from single-pass type 1 membrane proteins, and antigen source proteins in QIV were more likely to be secreted proteins **(Figure 3B).** Antigens in QIII were more likely to be from transcription factors, some of which have been previously reported to be ubiquitin-independent substrates *(reviewed in Jariel-Encontre et al., 2008).* Antigens in QIV were more likely to be produced from MHC Class II proteins; the ubiquitin-dependent, proteasome-independent degradation of these proteins isn't surprising *(Walseng, et al., 2010)*, although the immunological significance of these antigens is unclear.

Proteasome-dependent, ubiquitin-independent proteins in QIII warranted additional investigation given their surprising number. Source proteins for antigens in QIII did not appear to be more disordered as a whole **(Figure 3C)** or more likely to be from proteins classified as intrinsically disordered **(Supplemental Figure 3C)**, which has been reported to target proteins to the proteasome independent of ubiquitination *(Pena et al., 2009; Ngoc et al., 2014; Xia et al., 2019; Ukmar-Godec et al., 2020).* Peculiarly, the most striking feature of these proteins is that they are significantly shorter in length **(Figure 3C)**. The finding of a large collection of antigens more dependent on proteasomal degradation than ubiquitination is suggestive of degradation by proteasomes lacking 19S deubiquitinating enzyme caps, which does not directly require ubiquitination for protein degradation *(reviewed in Asher et al., 2006).*

Finally, we were interested in whether antigen generation generally requires the disaggregase p97/VCP. To test this, we treated cells with carfilzomib or the p97 inhibitor CB-5083 and assessed antigen presentation by mass spectrometry. As a whole, antigens appeared more dependent on proteasomal degradation than p97 for their generation **(Figure 3D)**, with less than one fourth of proteasome-dependent antigens found to also be p97-dependent **(Figure 3E)**. However, p97-dependent antigens were preferentially enriched in being derived from multiple types of membrane proteins, as compared with proteasome-dependent antigens **(Figure 3E).** This suggests the requirement of p97 in canonical

MHC Class I antigen generation may be limited mostly to proteins requiring extraction from membranes, including endoplasmic reticulum membrane proteins as expected *(Ye et al., 2001)*, although cross-presentation of exogenous antigens by specialized cell types may also be p97-dependent *(Menager et al., 2014).*

Atypical antigen presentation can be elicited by partial proteasome inhibition

While inhibition of ubiquitination or proteasomal degradation produces atypical antigens **(Figure 2D, E)**, sustained complete inhibition of these pathways across different tissue types is not clinically achievable. We considered whether partial inhibition of these pathways might be possible; for example, by inhibiting only the ubiquitination of certain proteins. Cullin-RING (CRL) E3 ligases are responsible for degradation of ~20% of proteins targeted by the proteasome *(Soucy et al., 2009)* and can be selectively inhibited. We treated cells with the neddylation inhibitor MLN4924 and the COP9 signalosome inhibitor CSN5i-3, both of which alter the activity of CRL E3 ligases **(Supplemental Figure 4A).** Neither treatment had a large impact on antigen presentation **(Supplemental Figure 4B),** although it is possible that CRL substrates may be lower in abundance and thus less likely to be detected as antigens by mass spectrometry. Nevertheless, we did observe that CSN5i-3 treatment increased presentation of CRL subunits and deneddylation components themselves as antigens **(Figure 4A)**. This effect of CSN5i-3 towards increasing presentation of antigens from these pathways, which is not unexpected given that CSN5i-3 promotes turnover of select CRL complexes *(Schlierf et al., 2016),* might have clinical applications in cancer patients with known mutations in these genes.

A method to elicit immunogenic antigen display in any patient, agnostic of mutation status, could have substantial clinical implications. We reasoned that this might be achievable via partial inhibition of the proteasome, if atypical antigens can be induced before dose-limiting toxicity is observed. Partial proteasome inhibition could also result in the production of antigens from previously antigenic proteins, but with alternative sequence constraints, due to decreased activity of certain proteasome active sites **(Supplemental Figure 4C)**. Treatment of cells with lower doses of carfilzomib that partially inhibited the proteasome **(Supplemental Figure 4D)** suggests that certain antigens could be induced **(Figure 4C)** before overall antigen presentation was reduced **(Figure 4B; Supplemental Figure 4E,F)**. Partial proteasome inhibition also induced the presentation of a smaller number of antigens not detected in vehicle treated cells **(Figure 4D)**; interestingly, this presentation was more striking with partial proteasome inhibition than near complete proteasome inhibition.

We reasoned that some of these antigens might be immunogenic; therefore, we were interested in whether they could appear in cells treated similarly to immune cells exposed to proteasome inhibitors in cancer patients. For subsequent experiments, we chose a dose of carfilzomib that inhibited the chymotrypsin-like site of the proteasome by approximately 75% **(Supplemental Figure 4G)**. This is comparable to the ≥75% inhibition of the chymotrypsin-like site observed in peripheral blood mononuclear cells of patients 1 h following carfilzomib treatment *(Lee et al., 2016)*. While activity of the remaining proteasome active sites (trypsin-like and caspase-like) should remain largely intact, and hence overall protein degradation may be only modestly impaired, we expect differential usage of proteasome active sites would alter the sequence of antigens displayed **(Supplemental Figure 4C)**.

We treated B lymphoblast cell lines for 48h with carfilzomib, or the immunoproteasome-specific chymotrypsin-like proteasome site inhibitor ONX-0914 *(Muchamuel et al., 2009)*, as immunoproteasomes are dominant in this cell line **(Supplemental Figure 4M).** Unlike how complete proteasome inhibition greatly reduces antigen display **(Supplemental Figure 2E, H)** we observed that antigen display was generally unchanged or mildly upregulated by partial proteasome inhibition

(Supplemental Figure 4H), although a smaller fraction of antigens was significantly decreased **(Supplemental Figure 4I)**. As expected, we observed that antigens significantly increased by proteasome inhibition, as compared to those decreased, had C-termini more likely to be produced by non-chymotrypsin-like proteasomal cleavage **(Supplemental Figure 4J,K)**.

While non-chymotrypsin-like antigens were more likely to be significantly increased by proteasome inhibition, most of these antigens were also detected in vehicle treated cells, and thus seem unlikely to be immunogenic. However, we were able to identify a small number of antigens only detected upon proteasome inhibition **(Figure 4E)**. As expected, these antigens were more likely to be produced by the non-chymotrypsin-like sites of the proteasome **(Supplemental Figure 4L)**. They were also more likely to not have been previously reported as MHC Class I antigens in the Immune Epitope Database *(Vita et al., 2019)* **(Figure 4F)**, hence increasing their likelihood of being immunogenic.

The idea that antigens produced by mild proteasome inhibition, like that observed clinically, are atypical enough to be immunogenic is difficult to reconcile with the fact that patients treated with these inhibitors do not appear to exhibit self-directed immune responses. However, proteasome inhibitors used clinically may also suppress the function of immune cells required for a response to atypical antigens. A fundamentally different approach would be to treat solid tumor cells, which are constitutive proteasome dominant, with a proteasome inhibitor that specifically inhibits only the constitutive proteasome and thus would have little effect on immune cells that contain high levels of immunoproteasome. In theory, this could induce immunogenic antigen display in a context where cytotoxic T cells and other immune cells are not negatively impacted by proteasome inhibitor treatment. To test this idea, we used HCC1954 breast cancer cells derived from the same patient as the HCC1954BL B lymphoblast cell line *(Gazdar et al., 1998)*. Unlike HCC1954BL, HCC1954 cells were not immunoproteasome-dominant, expressing approximately twice as many constitutive proteasome subunits as immunoproteasome subunits **(Supplemental Figure 4M)**. We aimed to treat these cells with carfilzomib, which targets constitutive and immunoproteasomes, as well as the immunoproteasome-specific inhibitor ONX-0914 and constitutive proteasome-specific inhibitor PR-825 *(Muchamuel et al., 2009; Winter et al., 2017)*, at doses mainly inhibiting the chymotrypsin-like site of the proteasome/immunoproteasome. As it is difficult to distinguish immunoproteasome versus constitutive proteasome inhibition *in vivo (Winter et al., 2017)*, we assumed complete specificity of ONX-0914 and PR-825 and estimated the percent of chymotrypsin-like proteasome activity inhibition to be indicative of immunoproteasome/constitutive proteasome composition based on immunoproteasome versus constitutive proteasome ratios **(Supplemental Figure 4N)**. Complete inhibition of the chymotrypsin-like site with carfilzomib was too toxic to obtain; however, we expect to have inhibited the chymotrypsin-like activity of the immunoproteasome or constitutive proteasome completely with ONX-0914 or PR-825, respectively, with minimal off-target activity **(Supplemental Figure 4O).**

HCC1954 cells were treated with these doses of carfilzomib, ONX-0914, and PR-825 for 48h and antigen presentation assessed by mass spectrometry. As in HCC1954BL cells, antigen presentation was not reduced by these inhibitors **(Supplemental Figure 4P)**; instead, presentation of select antigens was enhanced **(Figure 4G; Supplemental Figure 4Q)**, particularly with carfilzomib and PR-825 treatment. Also as observed in HCC1954BL cells, a smaller number of antigens was only detected in proteasome inhibitor treated cells **(Figure 4H)**. That these antigens were observed in PR-825 treated cells further suggests that partial proteasome inhibition using constitutive proteasome-specific inhibitors may enhance immunogenic antigen presentation in solid tumor cells, while minimizing potential negative impacts on effector immune cells.

DISCUSSION

MHC Class I antigens are selected from degradation products of endogenous proteins. Here, we systematically detail the contribution of protein degradation pathways to antigen generation. Specifically, we used mass spectrometry to quantitatively profile antigen presentation in response to perturbation of protein degradation. Technical optimizations were made to facilitate these investigations **(Figure 1)**, particularly inclusion of a spike-in MHC Class I antigen standard that is co-purified with antigens of interest for more accurate normalization. We also define a strategy to remove a considerable number of 'background antigens', antigens generally of low abundance not responsive to inhibitors that broadly block antigen presentation.

We then turned our attention towards the impact of ubiquitination and proteasomal degradation on antigen generation **(Figure 2)**. This question has been considered previously, by quantification of total levels of cell surface MHC Class I complexes and analysis of select model antigens following inhibition of these pathways *(Michalek et al., 1993; Rock et al., 1994; Wei et al., 2017)*. The contribution of the proteasome to antigen generation has also been defined in a semi-quantitative manner by mass spectrometry *(Kowalewski et al., 2016)*. Our experiments are the first to provide fully quantitative measurements for changes in presentation of thousands of antigens in response to inhibition of these pathways. We conclude that most – but not all – presented antigens require the proteasome (~70%) and ubiquitination (~60%) for their generation. Antigens that do not appear to require the ubiquitin-proteasome system are enriched in being derived from mitochondrial inner membrane proteins, which are normally inaccessible to proteasomes, although the mechanisms of their generation remain unclear. Another surprising finding is that a smaller number of antigens (~5%) are paradoxically increased by inhibition of these pathways. These antigens tend to be atypical, for example, being enriched in mitochondrial proteins (ubiquitination and proteasome inhibition) and single-pass transmembrane proteins (proteasome inhibition). Although compensatory autophagy can occur in response to decreased proteasomal activity *(Pandey et al., 2007),* autophagy did not appear to be the main source of most antigens increased by proteasome inhibition, as induction of these antigens was not reduced by the lysosomal protease inhibitor leupeptin or an ATG7 inhibitor. We also determined that antigens increased by proteasome inhibition do not appear to be loaded on the cell surface or within the endolysosomal system, arguing against a potential contribution from atypical antigen presentation pathways such as cross-presentation and MHC Class I recycling.

Another surprising finding is that close to 10% of antigens were found to be far more dependent on the proteasome than ubiquitination for their generation **(Figure 3)**. These antigens were enriched in being from transcription factors, which previous studies have suggested can serve as a source of ubiquitin-independent substrates *(reviewed in Jariel-Encontre et al., 2008)*. However, ubiquitination-independent antigens did not appear more likely to be derived from disordered proteins, another reported characteristic of ubiquitin-independent substrates *(Pena et al., 2009; Ngoc et al., 2014; Xia et al., 2019; Ukmar-Godec et al., 2020)*. Instead, a common finding is that these less ubiquitination-dependent antigens were derived from significantly shorter source proteins. The significance of this is unclear, although a clear preference for shorter proteins has been observed for monoubiqitination versus polyubiquitination *(Shabek et al., 2012; Braten el a., 2016)* and for proteins not ubiquitinated co-translationally *(Duttler et al., 2013)*. Co-translational protein ubiquitination is an interesting association given that co-translational protein degradation appears responsible for the rapid presentation of certain viral epitopes *(Croft et al., 2013).* However, the contribution of co-translational degradation versus degradation of stably folded proteins to antigen presentation under basal conditions remains controversial *(Yewdell et al., 1996; Schubert et al., 2000; Eisenlohr et al., 2007, Trentini et al., 2020)*.

A testable hypothesis is whether antigens less dependent on ubiquitination are produced by free 20S proteasomes, which generally outnumber 26S proteasomes *(Fabre et al., 2014).* Another potential contributor to antigen generation may by the disaggregase p97/VCP. We found that p97 is mostly required for generation of antigens from membrane proteins, as might be expected from its known roles in ER-associated degradation and membrane protein extraction *(reviewed in van den Boom, Meyer, 2018)*, although it may also be involved in cross-presentation of antigens from the endolysosomal system in specialized cell types *(Menager et al., 2014).*

We then wondered whether atypical antigen induction following protein degradation pathway inhibition could have therapeutic consequences. Complete and chronic inhibition of ubiquitination or the proteasome in humans is not achievable, as evidenced by severe autoinflammatory diseases associated with proteasome subunit or ubiquitination genetic losses *(Brehm et al., 2015; Beck et al., 2020)* and dose-limiting toxicity observed with clinical proteasome inhibitor use *(Aghajanian et al., 2002; O'Connor et al., 2009)*. However, inhibition of less broadly acting protein degradation pathways, such as certain E3 ligases, may be tolerated. We observed that antigens from predictable sources are increased by modulation of Cullin-RING E3 ligase activity, which may have clinical utility in patients with mutations in the corresponding genes.

However, a strategy to more broadly enhance presentation of antigens not limited to specific biological pathways is desirable. We considered partial proteasome inhibition **(Figure 4)**, which targets specific proteasome active sites, allowing the proteasome to retain degradative capacity, although with altered substrate sequence preferences. Partial proteasome inhibition did not result in cell death; it also did not decrease overall antigen presentation. In fact, certain antigens were increased in presentation by partial proteasome inhibition, particularly those produced by non-inhibited proteasome active sites. We were especially interested in antigens detected only in proteasome inhibitor treated cells, which were rare (generally <10 detected per cell line) but significantly more likely to not have been previously reported. We confirmed in a breast cancer cell line that proteasome inhibitor-specific antigens could be induced by proteasome inhibitors currently in the clinic (carfilzomib), as well as inhibitors selective for the immunoproteasome and constitutive proteasome (PR-825; *Muchamuel et al., 2009; Winter et al., 2017).* While selective inhibitors of the constitutive proteasome have not been developed for clinical usage, our results suggest these warrant attention for cancer immunotherapy applications, since alternative antigen display could be theoretically induced in solid tumor cells without impacting the viability or function of immunoproteasome-dominant effector immune cells.

In summary, a network of protein degradation pathways contributes to MHC Class I antigen production, although antigens from compensatory pathways are also observed when canonical pathways are disrupted **(Figure 5)**. Our studies identify new classes of protein degradation products; for example, proteasome-dependent, ubiquitin-independent substrates that are from significantly shorter source proteins. Additionally, we propose a new paradigm whereby partial inhibition of protein degradation pathways can elicit increased presentation of atypical antigens which may have applicability in cancer immunotherapy.

ACKNOWLEDGEMENTS

JLM was previously supported by a Life Sciences Research Foundation postdoctoral fellowship funded by Astellas Pharma and is currently supported by Amgen's Postdoctoral Fellows Program. At the outset of this work RJD was an Investigator of the Howard Hughes Medical Institute and was supported

therefrom. We thank Karl Beutner for insightful discussions on MHC Class I and Chris Spahr for help with initial mass spectrometry experiments. We thank Brett Lomenick, Spiros Garbis, and Tsui-Fen Chou from Caltech's Proteome Exploration Laboratory for running mass spectrometry experiments.

METHODS

Cell lines

HCC1143BL, HCC1954BL, HCC1395BL, HCC38BL, and HCC1954 *(Gazdar et al., 1998)* were purchased from ATCC and cultured in RPMI-1640 containing penicillin-streptomycin and 10% FBS. For experiments, B lymphoblast cell lines were used at a concentration of approximately 1E6 cells/ml.

For certain experiments using B lymphoblasts, cells were pre-treated with protein degradation inhibitors or vehicle for times indicated, and cell surface MHC Class I removed by acid stripping. This was accomplished by bathing approximately 2E7 cells in 10 mL acid stripping buffer (0.132M citric acid, 0.06M sodium phosphate, pH 3.0) for 2 min on ice, followed by neutralization in 40 mL ice cold medium. Cells were washed once in medium prior to experimental treatment.

Cells were collected for mass spec by centrifugation, which was preceded by trypsin detachment for adherent cell lines (HCC1954). Cell pellets were washed once in PBS and cell count and viability was assessed using a Vi-CELL XR.

Inhibitors

Carfilzomib, MLN4924, and CB-5083 were purchased from Selleck Chemical. MLN7243 was purchased from Chemie Tek. Cycloheximide was purchased from Sigma-Aldrich. Brefeldin A and leupeptin were purchased from Alfa Aesar. Cisplatin was purchased from R&D Systems. CSN5i-3 and ONX-0914 were purchased from Fisher. PR-825 and the ATG7 inhibitor, compound #37 *(Huang et al., 2020)*, were synthesized by WuXi AppTec.

Spike-in SIINFEKL standard

Mouse DC2.4 dendritic cells were purchased from Millipore and maintained in RPMI-1640 containing 10% FBS, penicillin-streptomycin, & L-glutamine. Purified SIINFEKL peptide from ovalbumin protein (AnaSpec) was added to cells at 25 µg/ml for 4h. Cells were washed in PBS and stored as frozen pellets for future mass spectrometry experiments.

Flow cytometry quantification of cell surface MHC Class I

Cells were washed twice in PBS. ~10E5 cells were resuspended in 100 µl 2% FBS in PBS with anti-MHC Class I antibody (W6/32-PE) at a 1:50 dilution. Cells were incubated at 4°C for 30 min, then washed three times in 2% FBS in PBS. Flow cytometry was performed on a BD Symphony (MHC Class I expression following acid stripping) or a BD LSR II (MHC Class I expression following MLN7243, carfilzomib, and cycloheximide treatment in HCC1143BL and HCC1954BL cells). Experiments were gated on single cells, and 10,000 events captured per sample. Median fluorescence intensity of PE was calculated by BD FACSDiva.

Proteasome activity assay

Approximately 5E5 cells were washed in PBS and lysed in 500 µl cold assay buffer [50 mM HEPES, pH 7.8, 10 mM NaCl, 1.5 mM $MgCl_2$, 1 mM EDTA, 1 mM EGTA, 250 mM sucrose, 5 mM DTT]. Cells were vortexed and sonicated for 5s at 50% power, then centrifuged at 14,000 rpm for 10 min at 4°C. 50 µl lysate was

loaded onto a 96 well plate on ice in triplicate for each proteasome activity probe. 200 µl assay buffer containing 2 mM ATP and 100 µM substrate (Suc-LLVY-AMC, Boc-LRR-AMC, Z-LLE-AMC, or Ac-nLPnLD-AMC) in DMSO was added to each well, and plates were incubated at 37°C for 1h. Plates were then imaged on a SpectraMax M5 fluorescent plate reader (excitation: 355 or 360 nM; emission: 460 nM). Fluorescence intensity was normalized to total protein content calculated by Bradford assay or total cell number.

Purification of MHC Class I antigens

MHC Class I antigens were purified from frozen samples based on a protocol described previously *(Chong et al., 2018)*. Prior to purification, anti-human MHC Class I antibody (W6/32; Bio X Cell) was crosslinked to protein A-sepharose 4B beads by incubation for 1h at room temperature with shaking, followed by crosslinking in 20 mM dimethyl pimelimidate dihydrocholoride, 0.1 M sodium borate for 30 min at room temperature. Equal parts 0.2M ethanolamine, pH 8 was added and mixed for 5 min. Solution was removed from beads and beads were incubated with 0.2M ethanolamine, pH 8 for 2h at room temperature. Beads were washed three times in PBS and stored in an equivalent volume of PBS with 0.02% sodium azide. Similarly, antibody against mouse MHC Class I/H-2K^{b} bound to SIINFEKL peptide (25-D1.16; Bio X Cell) was separately crosslinked to protein A-sepharose 4B beads. Anti-human MHC Class I antibody beads were mixed with anti-mouse MHC Class I-SIINFEKL beads at a 100:1 ratio. Approximately 1E7 frozen human cells were lysed in 1 mL cold lysis buffer [PBS with 0.25% sodium deoxycholate, 0.2 mM iodoacetamide, 1 mM EDTA, protease inhibitor cocktail, 1 mM PMSF, and 1% octyl-beta-D-glucopyranoside]. Frozen mouse cells presenting the SIINFEKL spike-in standard were also lysed in this buffer. Cells were lysed on ice with occasional vortexing for 30 min, then lysates centrifuged at 14,000 rpm for 30 min at 4°C. During this time, a 96 well filter plate was washed with 200 µl acetonitrile, 200 µl 0.1% formic acid, and 2x with 200 µl of 0.1M Tris-HCl, pH 8. Plates were centrifuged at 200 rpm for 1 min at 4°C if needed.

For each experiment, cleared lysate volumes representing an identical number of cells were used. These lysates were mixed with mouse cells presenting SIINFEKL peptide at a ratio of 100:1 cells. 150 µl of antibody slurry was added to wells of the 96 well filter plate and washed with 200 µl lysis buffer. Lysates were then passed through wells containing antibodies by gravity flow. Wells were washed 4x with 200 µl cold 150 mM NaCl in 20 mM Tris-HCl, pH 8, 4x with 200 µl cold 400 mM NaCl in 20 mM Tris-HCl, pH 8, 4x with 200 µl cold 150 mM NaCl in 20 mM Tris-HCl pH 8, and 2x with 200 µl cold 20 mM Tris-HCl pH 8. Plates were centrifuged at 200 rpm for 1 min at 4°C to pass wash buffers through plate. During this time, a Waters Sep-Pak tC18 96 well plate was washed with 1 mL 80% acetonitrile in 0.1% formic acid, followed by 2 mL 0.1% formic acid. MHC Class I complexes were eluted from the antibody plate into the C18 plate with 500 µl 1% trifluoroacetic acid. The C18 plate was washed with 2 mL 0.1% formic acid, and MHC Class I antigens eluted with 500 µl 28% acetonitrile in 0.1% formic acid.

Purified antigens were dried using a GeneVac vacuum evaporator, and resuspended in 100 mM HEPES, pH 8. Peptides were N-terminally labeled using TMT labels (10 samples: TMT10plex; 11 samples: TMT10plex + TMT11-131C; 12-16 samples: TMTpro), and combined for a single mass spectrometry run. Peptides were dried and desalted using C18 10 µl ZipTips before analysis.

LC-MS analysis using SPS-MS3

For most experiments, the entire sample was used for a single mass spectrometry run. Labelled peptides were subjected to LC-MS/MS analysis on an EASY 1000 nanoflow LC system coupled to a Fusion Tribrid Orbitrap mass spectrometer (Thermo Fisher Scientific) equipped with a Nanospray Flex ion source. Samples were directly loaded onto an Aurora 25cm x 75µm ID, 1.6µm C18 column (Ion Opticks) heated

to 50°C. The peptides were separated with a 2-hour gradient at 350 nL/min as follows: 2–6% Solvent B (7.5 min), 6-25% B (82.5 min), 25-40% B (30 min), 40-98% B (1 min), and held at 98% B (15 min). Solvent A consisted of 97.8 % H_2O, 2% ACN, and 0.2% formic acid and solvent B consisted of 19.8% H_2O, 80 % ACN, and 0.2% formic acid. The Fusion was operated in data dependent mode. Spray voltage was set to 2.2 kV, S-lens RF level at 60, and heated capillary at 275°C. Full scan resolution was set to 120,000 at m/z 200 in Profile mode with an AGC target of 4×10^5 and a maximum injection time of 50 ms. Precursor mass range was set to 400−1500 m/z and the isolation window was set to 0.7 m/z. For data dependent MS2 scans the cycle time was 3 sec, AGC target value was set at 5×10^4, and intensity threshold was kept at 5×10^3. CID fragmentation of precursors was performed with a fixed collision energy of 35%, activation time of 10 ms, and activation Q of 0.25. MS2 scans were then performed in the Orbitrap at 30,000 resolution in Centroid mode using auto scan range and a maximum injection time of 150ms. Dynamic exclusion was enabled to exclude after 2 times for 60 sec with a mass tolerance of 10 ppm. A charge state filter was also applied to only include precursors of charge 2-5. Quantitative MS3 scans were then performed using Multi-notch Isolation. SPS precursors were selected from the mass range of 400-1600 m/z with a precursor ion exclusion window from -50 to +5 m/z. Quadrupole isolation of the precursor used an isolation window of 0.7 m/z while the ms2 isolation window was set to 3 m/z for up to 10 notches. The AGC target was 5×10^4 and maximum injection time was set to 500 ms. HCD fragmentation was performed with fixed collision energy of 65% followed by Orbitrap detection at 50,000 resolution in Centroid mode using a scan range from 100-500 m/z.

Mass spectrometry data search

Raw data were analyzed in Proteome Discoverer 2.4 (Thermo Scientific) using an unspecific (no-enzyme) search with the Byonic search algorithm (Protein Metrics) and UniProt human fasta file containing the spike-in peptide sequence SIINFEKL. PD-Byonic search parameters were as follows: precursor mass tolerance of 5 ppm, CID low energy fragmentation, fragment mass tolerance of 20 ppm, and a maximum of 2 common modifications and 1 rare modification. Cysteine carbamidomethylation and TMT-6 or TMTpro addition to peptide N-termini and lysine were set as static modifications. Methionine oxidation was a common dynamic modification (up to 2 per peptide) and deamidated asparagine or glutamine was set as a rare dynamic modification (only 1 per peptide). Precursor and charge assignments were computed from MS1. Byonic protein-level FDR was set at 0.01, while Percolator FDRs were set at 0.001 (strict) and 0.01 (relaxed). In the consensus workflow, peptide and PSM FDRs were also set at 0.001 (strict) and 0.01 (relaxed), with peptide confidence at least medium, lower confidence peptides excluded, minimum peptide length set at 7, remove peptides without a protein reference set to false, and apply strict parsimony set to true. Quantification was performed at the ms3 level using reporter ion S/N ratios with an average reporter S/N threshold of 35, a co-isolation threshold of 30%, and an SPS mass matches threshold of 70%.

Mass spectrometry data statistical analysis

PSM output files from ProteomeDiscoverer were filtered for peptides not flagged in “Quan Info” as “ExcludedByMethod”. Only peptides 7-14 amino acids long were used. Peptides also needed to have an abundance; quantitation for at least 3 replicates of 1 treatment to be used. After this filtering, missing values were rare; when they occurred, values were imputed from a Gaussian distribution centered on the bottom 1^{st} peptide intensity percentile with standard deviation of the median standard deviation of peptides in the bottom 10^{th} intensity percentile. PSMs for identical peptides from the same UniProt ID were averaged. Peptide intensities were then normalized to the spike-in standard SIINFEKL intensity. A limma test was performed for statistical significance between treatments with R *(Ritchie et al., 2015)*. Results were considered significant when the adjusted p-value was < 0.01.

In certain experiments, an additional filter was applied: only peptides decreased at least 1.5 fold by cycloheximide treatment in both replicates. This filter was applied after the limma test was performed.

Heatmaps were generated using Seaborn's *clustermap* function with no column clustering in Python.

Peptide competition assay

Antigens previously identified to bind HLA-A*03:01 (TIAPALVSK) and HLA-B*35:03 (YPTTTISYL) in HCC38BL cells were purchased as ≥95% pure synthetic peptides from Sigma-Aldrich. These peptides were solubilized in DMSO and used for cell treatments at 20 ug/ml concentration, in the presence of absence of carfilzomib. Predicted antigen affinity scores were determined by NetMHCpan EL 4.1 ran by the Immune Epitope Database (IEDB). Only HLA-A*03:01 and HLA-B*35:03 were included in the search. The antigen was assigned to the HLA allele with the highest score.

Enrichment of subcellular localization and molecular function terms

The number of proteins associated with GO- Cellular Compartment and GO- Molecular Function terms was obtained from GeneTrail2 *(Stockel et al., 2016; Gene Ontology Consortium, 2021)*. Subcellular localization terms were also obtained from UniProt *(The UniProt Consortium, 2021).* Simplified subcellular localization terms were obtained from SubCellBarCode *(Orre et al., 2019).* Enrichment of terms for antigen nonredundant source proteins from one group of interest were compared with a second (e.g. nonredundant source proteins for antigens significantly increased by carfilzomib versus those significantly decreased). For experiments performed in a single cell line, enrichment of these terms was determined by Fisher's exact test with Bonferroni multiple testing corrections. At least 5 proteins needed to be associated with the term in at least one of the groups of antigens to be considered. For experiments performed in multiple cell lines, enrichment of these terms across cell lines was determined by Cochran–Mantel–Haenszel test with Bonferroni multiple testing corrections. At least 5 proteins across all cell lines needed to be associated with the term in at least one of the groups of antigens to be considered.

Enrichment of protein-protein interactions

Proteins reported to bind antigen source proteins were obtained from BioGRID *(Oughtred et al., 2021)*. Enrichment of interactors for antigen nonredundant source proteins from one group of interest were compared with a second (e.g. nonredundant source proteins for antigens significantly increased by carfilzomib versus those significantly decreased). Only low-throughput, physical interactors were used. Enrichment of these interactors across cell lines was determined by Cochran–Mantel–Haenszel test with Bonferroni multiple testing corrections. At least 5 proteins across all cell lines needed to be associated with the interactor in at least one of the groups of antigens to be considered.

Western blotting

Cells were lysed in NP40 lysis buffer [50 mM Tris-HCl, pH 7.4; 150 mM NaCl; 1% NP40] for the following experiments: treatment of cells with leupeptin, assessment of shRNA knockdown efficiency, and treatment of cells with MLN4924 and CSN5i-3. Cells were lysed in lysis buffer used for antigen mass spectrometry [PBS with 0.25% sodium deoxycholate, 0.2 mM iodoacetamide, 1 mM EDTA, protease inhibitor cocktail, 1 mM PMSF, and 1% octyl-beta-D-glucopyranoside] for the following experiments: dose and time response treatment with MLN7243 and treatment of cells with carfilzomib and MLN7423 during a cycloheximide chase. Protein concentration was determined by BCA assay (antigen mass spectrometry lysis buffer) or Bradford assay (NP40 lysis buffer). Equivalent protein amounts were run on Tris-Glycine gels and transferred to nitrocellulose membranes using Teknova Electroblot Buffer. Membranes were blocked in 5% milk and primary antibodies used at 1:1000 concentration.

Antibodies used were to polyubiquitin (FK1; Enzo BML-PW8805-0500), K48 polyubiquitin (Millipore 05-1307), ubiquitinated H2B (Cell Signaling 5546S), β-actin (Cell Signaling 3700S), LC3B (Cell Signaling 2775S), p62 (Cell Signaling 5114S), EIF4G1 (Cell Signaling 2469S), YTHDF2 (Proteintech 24744-1-AP), ARFGAP2 (Novus NBP1-83687), JUNB (Cell Signaling 3753S), ACSL4 (Invitrogen PA5-27137), IRF4 (Cell Signaling 4964S), GAPDH (Cell Signaling 5174T), PA28α (Abcam ab155091), PA28β (Cell Signaling 2409S), PA28γ (Cell Signaling 2412S), PA200 (Invitrogen PA1-1961), PI31 (Enzo BML-PW9710-0100), and CUL1 (Invitrogen 71-8700).

Flow cytometry measurement of apoptosis

HCC1954BL cells were treated with vehicle, 50 μM cisplatin, or 500 μM cisplatin for 20h, acid stripped to remove pre-existing MHC Class I complexes, and treated again with vehicle, 1 μM carfilzomib, 50 μM cisplatin, or 500 μM cisplatin for 4h. Approximately 1E6 cells were stained with Annexin V-FITC and propidium iodide (PI), staining apoptotic and dead cells, respectively, using a Life Technologies Dead Cell Apoptosis kit. Cutoffs for Annexin V-FITC and PI staining were established using unstained cells. Cells were classified as "live" (below the cutoff for Annexin V-FITC and PI staining), "early apoptotic" (above the cutoff for Annexin V-FITC staining), "late apoptotic/necrotic" (above the cutoff for Annexin V-FITC and PI staining), and "other". Experiments were gated on single cells, and 10,000 events captured per sample on a BD Symphony. Analysis was performed with FACSDiva.

Fluorescent proteasome gels

1h prior to cell harvesting, cells were treated with 500 nM Me4BodipyFL-Ahx3Leu3VS. Cells were washed with PBS during harvesting and lysed in cold NP40 lysis buffer [50 mM Tris-HCl, pH 7.4, 150 mM NaCl, 1% NP40, & protease inhibitor cocktail]. Cells were lysed at 4°C for 30 min with rotation and centrifuged at 14,000 rpm for 5 min at 4°C. 10 μg of protein was loaded onto 16% Tricine SDS-PAGE gels and run for approximately 4-6h at 120 V with Tricine running buffer containing 1:400 NuPAGE antioxidant. Gels were imaged on a Typhoon FLA9500 fluorescent gel scanner (excitation: 473 nm; emission filter: BPB1 530DF20).

Enrichment of deneddylation and Cullin-RING ligase terms after CSN5i-3 treatment

Proteins with deneddylation gene ontology terms were obtained from UniProt *(The UniProt Consortium, 2021)* in November 2021. Proteins listed as Cullin-RING ligases (CRL) were obtained from UUCD *(Gao et al., 2013)*. Nonredundant source proteins for peptides significantly increased by CSN5i-3 treatment were compared with nonredundant source proteins for peptides not significantly changed by CSN5i-3 treatment. Enrichment of these terms in peptides significantly increased by CSN5i-3 treatment was determined by Fisher's exact test with Bonferroni multiple testing corrections.

Proteasome cleavage site prediction

The C-terminal amino acid was determined for antigens and classified as "chymotrypsin-like" (alanine, phenylalanine, isoleucine, leucine, methionine, valine, tryptophan, or tyrosine), "trypsin-like" (lysine or arginine), or "other" (all other amino acids) *(Kisselev 2003)*. Enrichment of trypsin-like antigens in antigens increased by ONX-0914 versus those decreased was determined by Fisher's exact test. Enrichment of trypsin-like antigens in antigens only detected after proteasome inhibitor treatment across all cell lines was determined by Cochran–Mantel–Haenszel test.

Calculation of antigen source protein length and disorder

Antigen source protein length was obtained from UniProt *(The UniProt Consortium, 2021)*. The percent instability of antigen source proteins was obtained from Dryad (*Vincent, Schnell, 2016; Vincent, Schnell, 2017).* Significance of differences in length and percent disorderbetween nonredundant proteins in QIII

and those decreased by MLN7243 and carfilzomib treatment across all cell lines was determined by Fisher's method combining t-test p-values from each cell line. Number of antigen source proteins considered to be intrinsically disordered was obtained from DisProt *(Hatos et al., 2020)*. Significance of differences in fraction of nonredundant antigen source proteins characterized as intrinsically disordered in QIII versus those decreased by MLN7243 and carfilzomib treatment ("UPS-dependent") across all cell lines was determined by Cochran–Mantel–Haenszel test.

REFERENCES

Aghajanian C, Soignet S, Dizon DS, Pien CS, Adams J, Elliott PJ, Sabbatini P, Miller V, Hensley ML, Pezzulli S, Canales C, Daud A, Spriggs DR. 2002. A Phase I Trial of the Novel Proteasome Inhibitor PS341 in Advanced Solid Tumor Malignancies. *Clin Cancer Res* **8(8)**: 2505-2511.

Asher G, Reuven N, Shaul Y. 2006. 20S Proteasomes and Protein Degradation "By Default". *Bioessays* **28(8)**: 844-849.

Beck DB, Ferrada MA, Sikora KA, Ombrello AK, Collins JC, Pei W, Balanda N, Ross DL, Cardona DO, Wu Z, Patel B, Manthiram K, Groarke EM, Gutierrez-Rodrigues F, Hoffmann P, Rosenzweig S, Nakabo S, Dillon LW, Hourigan CS, Tsai WL, Gupta S, Carmona-Rivera C, Asmar AJ, Xu L, Oda H, Goodspeed W, Barron KS, Nehrebecky M, Jones A, Laird RS, Deuitch N, Rowczenio D, Rominger E, Wells KV, Lee CR, Wang W, Trick M, Mullikin J, Wigerblad G, Brooks S, Dell'Orso S, Deng Z, Chae JJ, Dulau-Florea A, Malicdan MCV, Novacic D, Colbert RA, Kaplan MJ, Gadina M, Savic S, Lachmann HJ, Abu-Asab M, Solomon BD, Retterer K, Gahl WA, Burgess SM, Aksentijevich I, Young NS, Calvo KR, Werner C, Kastner DL, Grayson PC. 2020. Somatic Mutations in UBA1 and Severe Adult-Onset Autoinflammatory Disease. *N Engl J Med* **383(27)**: 2628-2638.

Braten O, Livneh I, Ziv T, Admon A, Kehat I, Caspi LH, Gonen H, Bercovich B, Godzik A, Jahandideh S, Jaroszewski L, Sommer T, Kwon YT, Guharoy M, Tompa P, Ciechanover A. 2016. Numberous Proteins with Unique Characteristics are Degraded by the 26S Proteasome Following Monoubiquitination. *Proc Natl Acad Sci U S A* **113(32)**: E4639-E4647.

Brehm A, Liu Y, Sheikh A, Marrero B, Omoyinmi E, Zhou Q, Montealegre G, Biancotto A, Reinhardt A, Almeida de Jesus A, Pelletier M, Tsai WL, Remmers EF, Kardava L, Hill S, Kim H, Lachmann HJ, Megarbane A, Chae JJ, Brady J, Castillo RD, Brown D, Casano AV, Gao L, Chapelle D, Huang Y, Stone D, Chen Y, Sotzny F, Lee CR, Kastner DL, Torrelo A, Zlotogorski A, Moir S, Gadina M, McCoy P, Wesley R, Rother KI, Hildebrand PW, Brogan P, Kruger E, Aksentijevich I, Goldbach-Mansky R. 2015. Additive Loss-of-Function Proteasome Subunit Mutations in CANDLE/PRAAS Patients Promote Type 1 IFN Production. *J Clin Invest* **125(11)**: 4196-4211.

Chong C, Marino F, Pak H, Racle J, Daniel RT, Muller M, Gfeller D, Coukos G, Bassani-Sternberg M. 2018. High-throughput and Sensitive Immunopeptidomics Platform Reveals Profound Interferonγ-Mediated Remodeling of the Human Leukocyte Antigen (HLA) Ligandome. *Mol Cell Proteomics* **17(3)**: 533-548.

Cox JH, Yewdell JW, Eisenlohr LC, Johnson PR, Bennink JR. 1990. Antigen Presentation Requires Transport of MHC Class I Molecules from the Endoplasmic Reticulum. *Science* **247(4943)**: 715-718.

Croft NP, Smith SA, Wong YC, Tan CT, Dudek NL, Flesch IEA, Lin LCW, Tscharke DC, Purcell AW. 2013. Kinetics of Antigen Expression and Epitope Presentation during Virus Infection. *PLoS Pathog* **9(1)**: e1003129.

Duttler S, Pechmann S, Frydman J. 2013. Principles of Cotranslational Ubiquitination and Quality Control at the Ribosome. *Mol Cell* **50(3)**: 379-393.

Eisenlohr LC, Huang L, Golovina TN. 2007. Rethinking Peptide Supply to MHC Class I Molecules. *Nat Rev Immunol* **7(5)**: 403-410.

Fabre B, Lambour T, Garrigues L, Ducoux-Petit M, Amalric F, Monsarrat B, Burlet-Schiltz O, Bousquet-Dubouch M-P. 2014. Label-Free Quantitative Proteomics Reveals the Dynamics of Proteasome Complexes Composition and Stoichiometry in a Wide Range of Human Cell Lines. *J Proteome Res* **13(6)**: 3027-3037.

Gao T, Liu Z, Wang Y, Cheng H, Yang Q, Guo A, Ren J, Xue Y. 2013. UUCD: A Family-Based Database of Ubiquitin and Ubiquitin-Like Conjugation. *Nucleic Acids Res* **41(Database Issue)**: D445-D451.
Gene Ontology Consortium. 2021. The Gene Ontology Resource: Enriching a GOld Mine. *Nucleic Acids Res* **49(D1)**: D325-D334.

Gazdar AF, Kurvari V, Virmani A, Gollahon L, Sakaguchi M, Westerfield M, Kodagoda D, Stasny V, Cunningham HT, Wistuba II, Tomlinson G, Tonk V, Ashfaq R, Leitch AM, Minna JD, Shay JW. 1998. Characterization of Paired Tumor and Non-Tumor Cell Lines Established from Patients with Breast Cancer. *Int J Cancer* **78(6)**: 766-774.

Hatos A, Hajdu-Soltesz B, Monzon AM, Palopoli N, Alvarez L, Aykac-Fas B, Bassot C, Benitez GI, Bevilacqua M, Chasapi A, Chemes L, Davey NE, Davidovic R, Dunker AK, Elofsson A, Gobeill J, Foutel NSG, Sudha G, Guharoy M, Horvath T, Iglesias V, Kajava AV, Kovacs OP, Lamb J, Lambrughi M, Lazar T, Leclercq JY, Leonardi E, Macedo-Ribeiro S, Macossay-Castillo M, Maiani E, Manso JA, Marino-Buslje C, Martínez-Pérez E, Meszaros B, Micetic I, Minervini G, Murvai N, Necci M, Ouzounis CA, Pajkos M, Paladin L, Pancsa R, Papaleo E, Parisi G, Pasche E, Pereira PJB, Promponas VJ, Pujols J, Quaglia F, Ruch P, Salvatore M, Schad E, Szabo B, Szaniszlo T, Tamana S, Tantos A, Veljkovic N, Ventura S, Vranken W, Dosztanyi Z, Tompa P, Tosatto SCE, Piovesan D. 2020. DisProt: Intrinsic Protein Disorder Annotation in 2020. *Nucleic Acids Res* **48(D1)**: D269-D276.

Huang S-C, Adhikari S, Brownell JE, Calderwood EF, Chouitar J, D'Amore NR, England DB, Foley K, Harrison SJ, LeRoy PJ, Lok D, Lublinsky A, Ma L-T, Menon S, Yang Y, Zhang J, Gould AE. 2020. Discovery and Optimization of Pyrazolopyrimidine Sulfamates as ATG7 Inhibitors. *Bioorg Med Chem* **28(19):** 115681.

Jariel-Encontre I, Bossis G, Piechaczyk M. 2008. Ubiquitin-Independent Degradation of Proteins by the Proteasome. *Biochim Biophys Acta* **1786(2)**: 153-177.

Ke Y, Kapp JA. 1996. Exogenous Antigens Gain Access to the Major Histocompatibility Complex Class I Processing Pathway in B Cells by Receptor-Mediated Uptake. *J Exp Med* **184(3)**: 1179-1184.

Kisselev AF, Garcia-Calvo M, Overkleeft HS, Peterson E, Pennington MW, Ploegh HL, Thornberry NA, Goldberg AL. 2003. The Caspase-Like Sites of Proteasomes, Their Substrate Specificity, New Inhibitors

and Substrates, and Allosteric Interactions with the Trypsin-Like Sites. *J Biol Chem* **278(38)**: 35869-35877.

Kisselev AF, Callard A, Goldberg AL. 2006. Importance of the Different Proteolytic Sites of the Proteasome and the Efficacy of Inhibitors Varies with the Protein Substrate. *J Biol Chem* **281(13)**: 8582-8590.

Kowalewski DJ, Walz S, Backert L, Schuster H, Kohlbacher O, Weisel K, Rittig SM, Kanz L, Salih HR, Rammensee H-G, Stevanovic S, Stickel JS. 2016. Carfilzomib Alters the HLA-Presented Peptidome of Myeloma Cells and Impairs Presentation of Peptides with Aromatic C-Termini. *Blood Cancer J* **6(4)**: e411.

Lee SJ, Levitsky K, Parlati F, Bennett MK, Arastu-Kapur S, Kellerman L, Woo TF, Wong AF, Papadopoulos KP, Nievizky R, Badros AZ, Vij R, Jagannath S, Siegel D, Wang M, Ahmann GJ, Kirk CJ. 2016. Clinical Activity of Carfilzomib Correlates with Inhibition of Multiple Proteasome Subunits: Application of a Novel Pharmacodynamic Assay. *Br J Haematol* **173(6):** 884-895.

Lundegaard C, Lund O, Buus S, Nielsen M. 2010. Major Histocompatibility Complex Class I Binding Predictions as a Tool in Epitope Discovery. *Immunology* **130(3)**: 309-318.

McMahon M, Ding S, Acosta-Jimenez LP, Frangova TG, Henderson CJ, Wolf CR. 2018. Measuring In Vivo Responses to Endogenous and Exogenous Oxidative Stress Using a Novel Haem Oxygenase 1 Reporter Mouse. *J Physiol* **596(1)**: 105-127.

Menager J, Ebstein F, Oger R, Hulin P, Nedellec S, Duverger E, Lehmann A, Kloetzel P-M, Jotereau F, Guilloux Y. 2014. Cross-Presentation of Synthetic Long Peptides by Human Dendritic Cells: A Process Dependent on ERAD Component p97/VCP but Not Sec61 and/or Derlin-1. *PLoS One* **9(2)**: e89897.

Michalek MT, Grant EP, Gramm C, Goldberg AL, Rock KL. 1993. A Role for the Ubiquitin-Dependent Proteolytic Pathway in MHC Class I-Restricted Antigen Presentation. *Nature* **363(6429)**: 552-554.

Montealegre S, Venugopalan V, Fritzsche S, Kulicke C, Hein Z, Springer S. 2015. Dissociation of β2-Microglobulin Determines the Surface Quality Control of Major Histocompatibility Complex Class I Molecules. *FASEB J* **29(7):** 2780-2788.

Muchamuel T, Basler M, Aujay MA, Suzuki E, Kalim KW, Lauer C, Sylvain C, Ring ER, Shields J, Jiang J, Shwonek P, Parlati F, Demo SD, Bennett MK, Kirk CJ, Groettrup M. 2009. A Selective Inhibitor of the Immunoproteasome Subunit LMP7 Blocks Cytokine Production and Attenuates Progression of Experimental Arthritis. *Nat Med* **15(7)**: 781-787.

Murakami Y, Matsufuji S, Kameji T, Hayashi S, Igarashi K, Tamura T, Tanaka K, Ichihara A. 1992. Ornithine Decarboxylase is Degraded by the 26S Proteasome Without Ubiquitination. *Nature* **360(6404)**: 597-599.

Ngoc LV, Wauquier C, Soin R, Bousbata S, Twyffels L, Kruys V, Gueydan C. 2014. Rapid Proteasomal Degradation of Posttranscriptional Regulators of the TIS11/Tristetraprolin Family is Induced by an Intrinsically Unstructured Region Independently of Ubiquitination. *Mol Cell Biol* **34(23)**: 4315-4328.
O'Connor OA, Stewart AK, Vallone M, Molineaux CJ, Kunkel LA, Gerecitano JF, Orlowski RZ. 2009. A Phase I Dose Escalation Study of the Safety and Pharmacokinetics of the Novel Proteasome Inhibitor Carfilzomib (PR-171) in Patients with Hematologic Malignancies. *Clin Cancer Res* **15(22)**: 7085-7091.

Orre LM, Vesterlund M, Pan Y, Arslan T, Zhu Y, Woodbridge AF, Frings O, Fredlund E, Lehtio J. 2019. SubCellBarCode: Proteome-Wide Mapping of Protein Localization and Relocalization. *Mol Cell* **73(1)**: 166-182.

Oughtred R, Rust J, Chang C, Breitkreutz B-J, Stark C, Willems A, Boucher L, Leung G, Kolas N, Zhang F, Dolma S, Coulombe-Huntington J, Chatr-Aryamontri A, Dolinski K, Tyers M. 2021. The BioGRID Database: A Comprehensive Biomedical Resource of Curated Protein, Genetic, and Chemical Interactions. *Protein Sci* **30(1)**: 187-200.

Pandey UB, Nie Z, Batlevi Y, McCray BA, Ritson GP, Nedelsky NB, Schwartz SL, DiProspero NA, Knight MA, Schuldiner O, Padmanabhan R, Hild M, Berry DL, Garza D, Hubbert CC, Yao T-P, Baehrecke EH, Taylor JP. 2007. HDAC6 Rescues Neurodegeneration and Provides an Essential Link between Autophagy and the UPS. *Nature* **447(7146)**: 859-863.

Pena MM, Melo SP, Xing YY, White K, Barbour KW, Berger FG. 2009. The Intrinsically Disordered N-Terminal Domain of Thymidylate Synthase Targets the Enzyme to the Ubiquitin-Independent Proteasomal Degradation Pathway. *J Biol Chem* **284(46)**: 31597-31607.

Raiborg C, Bache KG, Gillooly DJ, Madshus IH, Stang E, Stenmark H. 2002. Hrs Sorts Ubiquitinated Proteins into Clathrin-Coated Microdomains of Early Endosomes. *Nat Cell Biol* **4(5)**: 394-398.

Ritchie ME, Phipson B, Wu D, Hu Y, Law CW, Shi W, Smyth GK. 2015. Limma Powers Differential Expression Analyses for RNA-Sequencing and Microarray Studies. *Nucleic Acids Res* **43(7)**: e47.

Rock KL, Gramm C, Rothstein L, Clark K, Stein R, Dick L, Hwang D, Goldberg AL. 1994. Inhibitors of the Proteasome Block the Degradation of Most Cell Proteins and the Generation of Peptides Presented on MHC Class I Molecules. *Cell* **78(5)**: 761-771.

Rock KL, Reits E, Neefjes J. 2016. Present Yourself! By MHC Class I and MHC Class II Molecules. *Trends Immunol* **37(11)**: 724-737.

Saeki Y. 2017. Ubiquitin Recognition by the Proteasome. *J Biochem* **161(2)**: 113-124.

Schlierf A, Altmann E, Quancard J, Jefferson AB, Assenberg R, Renatus M, Jones M, Hassiepen U, Schaefer M, Kiffe M, Weiss A, Wiesmann C, Sedrani R, Eder J, Martoglio B. 2016. Targeted Inhibition of the COP9 Signalosome for Treatment of Cancer. *Nat Commun* **7:** 13166.

Schmidt A, Gehlenborg N, Bodenmiller B, Mueller LN, Campbell D, Mueller M, Aebersold R, Domon B. 2008. An Integrated, Directed Mass Spectrometric Approach for In-Depth Characterization of Complex Peptide Mixtures. *Mol Cell Proteomics* **7(11)**: 2138-2150.

Schubert U, Anton LC, Gibbs J, Norbury CC, Yewdell JW, Bennink JR. 2000. Rapid Degradation of a Large Fraction of Newly Synthesized Proteins by Proteasomes. *Nature* **404(6779)**: 770-774.

Shabek N, Herman-Bachinsky Y, Buchsbaum S, Lewinson O, Haj-Yahya M, Hejjaoui M, Lashuel HA, Sommer T, Brik A, Ciechanover A. 2012. The Size of the Proteasomal Substrate Determines Whether its Degradation Will Be Mediated by Mono- or Polyubiquitylation. *Mol Cell* **48(1)**: 87-97.

Soucy TA, Smith PG, Milhollen MA, Berger AJ, Gavin JM, Adhikari S, Brownell JE, Burke KE, Cardin DP, Critchley S, Cullis CA, Doucette A, Garnsey JJ, Gaulin JL, Gershman RE, Lublinsky AR, McDonald A, Mizutani H, Narayanan U, Olhava EJ, Peluso S, Rezaei M, Sintchak MD, Talreja T, Thomas MP, Traore T, Vyskocil S, Weatherhead GS, Yu J, Zhang J, Dick LR, Claiborne CF, Rolfe M, Bolen JB, Langston SP. 2009. An Inhibitor of NEDD8-Activating Enzyme as a New Approach to Treat Cancer. *Nature* **458(7239)**: 732-736.

Stockel D, Kehl T, Trampert P, Schneider L, Backes C, Ludwig N, Gerasch A, Kaufmann M, Gessler M, Graf N, Meese E, Keller A, Lenhof H-P. 2016. Multi-Omics Enrichment Analysis Using the GeneTrail2 Web Service. *Bioinformatics* **32(10)**: 1502-1508.

Sugawara S, Abo T, Kumagai K. 1987. A Simple Method to Eliminate the Antigenicity of Surface Class I MHC Molecules from the Membrane of Viable Cells by Acid Treatment at pH 3. *J Immunol Methods* **100(1-2)**: 83-90.

Trentini DB, Pecoraro M, Tiwary S, Cox J, Mann M, Hipp MS, Hartl FU. 2020. Role for Ribosome-Associated Quality Control in Sampling Proteins for MHC Class I-Mediated Antigen Presentation. *Proc Natl Acad Sci USA* **117(8)**: 4099-4108.

The UniProt Consortium. 2021. UniProt: The Universal Protein Knowledgebase in 2021. *Nucleic Acids Res* **49(D1)**: D480-D489.

Ukmar-Godec T, Fang P, Ibanez de Opakua A, Henneberg F, Godec A, Pan K-T, Cima-Omori M-S, Chari A, Mandelkow E, Urlaub H, Zweckstetter M. 2020. Proteasomal Degradation of the Intrinsically Disordered Protein Tau at Single-Residue Resolution. *Sci Adv* **6(30)**: eaba3916.

van den Boom J, Meyer H. 2018. VCP/p97-Mediated Unfolding as a Principle in Protein Homeostasis and Signaling. *Mol Cell* **69(2)**: 182-194.

Vincent M, Schnell S. 2016. A Collection of Intrinsic Disorder Characteristics from Eukaryotic Proteomes. *Sci Data* **3:** 160045.

Vincent M, Schnell S. 2017. Data From: A Collection of Intrinsic Disorder Characteristics from Eukaryotic Proteomes. Dryad, Dataset, https://doi.org/10.5061/dryad.sm107.

Vita R, Mahajan S, Overton JA, Dhanda SK, Martini S, Cantrell JR, Wheeler DK, Sette A, Peters B. 2019. The Immune Epitope Database (IEDB): 2018 Update. *Nucleic Acids Res* **47(D1):** D339-D343.

Wang J, Sun H-Q, Macia E, Kirchhausen T, Watson H, Bonifacino JS, Yin HL. 2007. PI4P Promotes the Recruitment of the GGA Adaptor Proteins to the Trans-Golgi Network and Regulates Their Recognition of the Ubiquitin Sorting Signal. *Mol Biol Cell* **18(7)**: 2646-2655.

Wei J, Zanker D, Di Carluccio AR, Smelkinson MG, Takeda K, Seedhom MO, Dersh D, Gibbs JS, Yang N, Jadhav A, Chen W, Yewdell JW. 2017. Varied Role of Ubiquitylation in Generating MHC Class I Peptide Ligands. *J Immunol* **198(10):** 3835-3845.

Winter MB, La Greca F, Arastu-Kapur S, Caiazza F, Cimermancic P, Buchholz TJ, Anderl JL, Ravalin M, Bohn MF, Sali A, O'Donoghue AJ, Craik CS. 2017. Immunoproteasome Functions Explained by Divergence in Cleavage Specificity and Regulation. *Elife* **6:** e27364.

Xia T, Yi XM, Wu X, Shang J, Shu HB. 2019. PTPN1/2-Mediated Dephosphorylation of MITA/STING Promotes Its 20S Proteasomal Degradation and Attenuates Innate Antiviral Response. *Proc Natl Acad Sci U S A* **116(40)**: 20063-20069.

Ye Y, Meyer HH, Rapoport TA. 2001. The AAA ATPase Cdc48/p97 and its Partners Transport Proteins from the ER into the Cytosol. *Nature* **414(6864)**: 652-656.

Yewdell JW, Anton LC, Bennink JR. 1996. Defective Ribosomal Products (DRIPs): A Major Source of Antigenic Peptides for MHC Class I Molecules? *J Immunol* **157(5)**: 1823-1826.

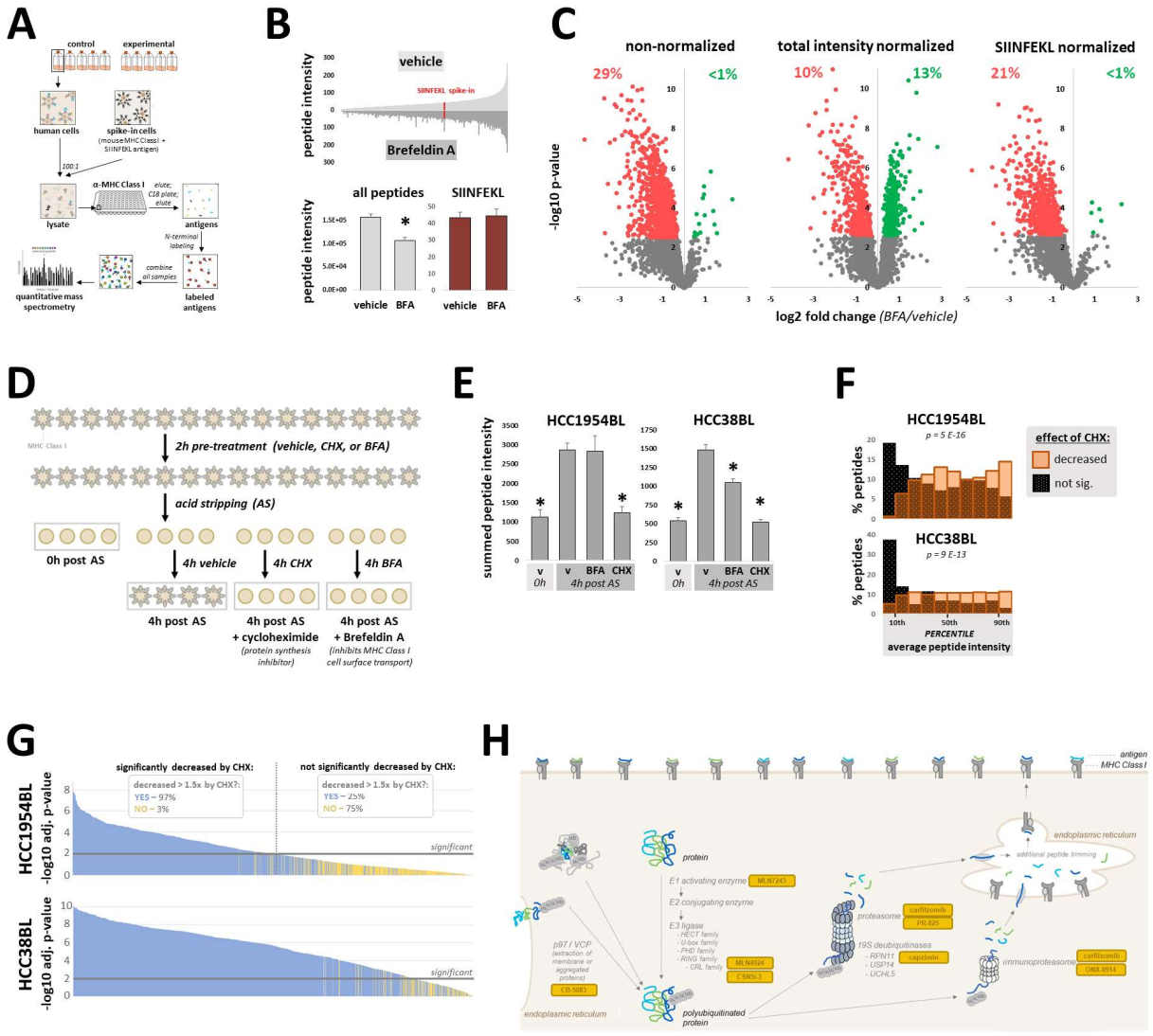

Figure 1. MHC Class I antigen mass spectrometry is improved by methodology for more accurate data normalization and removal of 'background antigens'. (A) Experimental design for mass spectrometry quantification of MHC Class I antigens in response to treatment. **(B)** Top: Waterfall plots of average mass spectrometry signal intensity of peptides captured from vehicle (upper) and brefeldin A (BFA)(lower; 5 µM for 16h) treated HCC1954BL cells (n=5/group). SIINFEKL spike-in peptide is marked in red. Bottom: fSummed peptide intensity and SIINFEKL spike-in peptide intensity quantified by mass spectrometry for cells treated with brefeldin A (BFA) or vehicle. Graph represents average + SEM; * denotes $p < 0.01$ by t-test. **(C)** Volcano plots representing quantitative changes in MHC Class I peptides upon BFA treatment (red indicates significantly decreased by limma test; green indicates significantly increased). Data are presented as non-normalized, total intensity normalized (each sample normalized to its summed peptide intensity), and normalized to the spike-in SIINFEKL peptide. Percent significant (increased and decreased) are marked above plots. **(D)** Experimental design for treatment of cells to block MHC Class I antigen presentation. Cells were pre-treated with vehicle (v), cycloheximide (CHX; 25µg/ml), or BFA (5 µM) for 2h, and pre-existing MHC Class I-bound antigen peptides removed by mild acid elution ("acid stripping"; AS). Cells were immediately collected after AS, or treated again with vehicle, cycloheximide, or BFA for 4h. Expected impact of treatments on MHC Class I antigen presentation is depicted. **(E)**

Summed peptide intensity quantified by mass spectrometry for two B lymphoblast cell lines treated as described in Figure 1D. Graph represents average + SEM (n=4 for all groups). * indicates $p < 0.01$, as compared with 4h post AS + vehicle, by Dunnett's test. **(F)** Significance of treatments as described in Figure 1D was determined by limma test. The average peptide intensity at 4h post acid stripping, representing constitutive antigen presentation, was determined for two groups: antigens significantly decreasing in response to CHX treatment, and those not significantly decreasing. Average peptide intensity percentiles were determined and presented as histograms; p-value was determined by t-test of average peptide intensities. **(G)** Similar to Figure 1F, the following groups were compared: antigens significantly decreasing in response to cycloheximide CHX treatment, and those not significantly decreasing. Waterfall plots of the –log10(adjusted p-value), as determined by limma test, are shown. Another comparison using this dataset was performed, which involves using just the first 2 replicates of the CHX treatment group (n=4 previously). Antigens decreased greater than 1.5 fold in response to CHX in both replicates (n=2) versus vehicle are plotted in blue, with all others plotted in yellow. In the legend, "decreased > 1.5 fold by CHX" means decreased > 1.5 fold by CHX in both replicates (n=2). Percentages of antigens decreased by CHX listed are for HCC1954BL cells. **(H)** Protein degradation pathways to be systematically assessed for an impact on MHC Class I antigen presentation. Protein degradation pathway inhibitors are marked in yellow boxes.

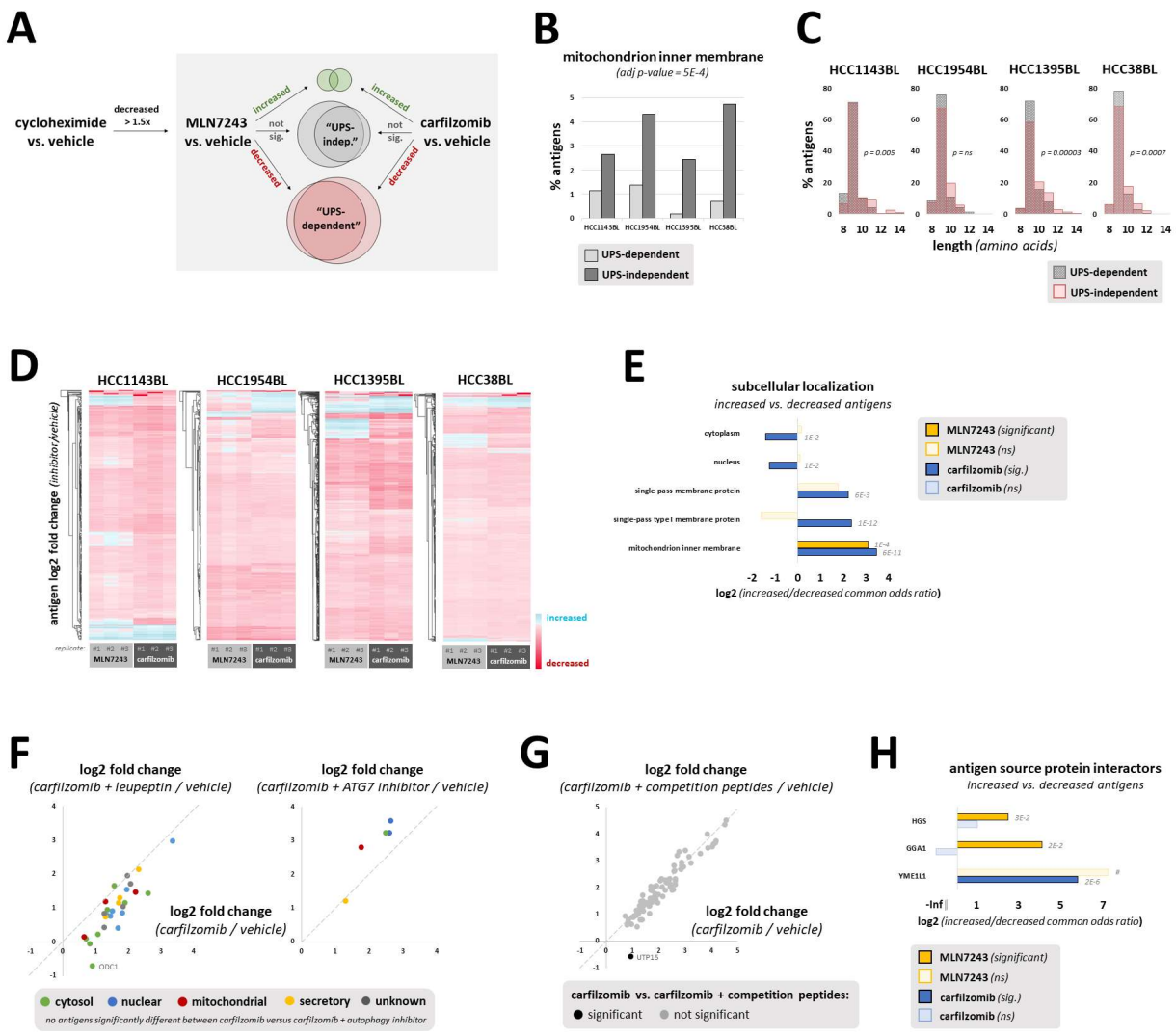

Figure 2. Inhibition of ubiquitination and proteasomal degradation results in a net decrease in antigen presentation, yet paradoxical increases in certain antigens. **(A)** Criteria for classification of "ubiquitin-proteasome system (UPS)-dependent" and "UPS-independent" antigens. Venn diagrams are proportionally accurate.(**B)** Enrichment of mitochondrial inner membrane proteins as source of antigens not significantly decreased by MLN7243 and carfilzomib ("UPS-independent") versus those significantly decreased by MLN7243 and carfilzomib ("UPS-dependent"). Cells were treated with MLN7243 (500 nM; 4h pretreatment), carfilzomib (1 μM; 1h pretreatment), or cycloheximide (25 μg/ml; 2h pretreatment) for 4h following acid stripping. Limma test was performed for significance, and antigens not decreasing more than 1.5 fold in response to cycloheximide (n=2) in both replicates were subsequently excluded. n=3 for vehicle, MLN7243, and carfilzomib treatments in each cell line. Subcellular localization for UPS-independent and UPS-dependent antigens was obtained from UniProt, and the Cochran–Mantel–Haenszel test was used to test the enrichment of subcellular localization terms across all cell lines. **(C)** Histogram of antigen length (# amino acids) for antigens not significantly decreased by MLN7243 and carfilzomib ("UPS-independent") versus those significantly decreased by MLN7243 and carfilzomib ("UPS-dependent"). Cells were treated as in Figure 2B. **(D)** Heat map of antigens increased (blue) or decreased (red) by MLN7243 and carfilzomib treatment. Cells were treated as in Figure 2B. Heat map shows log2 fold change (inhibitor/vehicle), and only includes antigens significant in at least one

treatment. **(E)** Enrichment of subcellular localization gene ontology terms in antigens significantly increased versus antigens significantly decreased in cells treated with MLN7243 or carfilzomib. Cells were treated as in Figure 2B. Subcellular localization for antigens significantly increased and antigens significantly decreased by MLN7243 and carfilzomib was obtained from UniProt. The Cochran–Mantel–Haenszel test was used to test the enrichment of subcellular localization terms across all cell lines. Bonferroni corrected adjusted p-values are indicated for significantly enriched terms. Sig, significant; ns, non-significant. **(F)** HCC1954BL cells were treated with carfilzomib (1 μM; 1h pretreatment), leupeptin (50 μM; 1h pretreatment), carfilzomib & leupeptin (1 μM & 50 μM, respectively; 1h pretreatment) and cycloheximide (25 μg/ml; 2h pretreatment) for 4h following acid stripping. n=3 for vehicle, leupeptin, and carfilzomib treatments. Similarly, HCC1954BL cells were treated with carfilzomib (1 μM; 1h pretreatment), ATG7 inhibitor (25 μM; 1h pretreatment), carfilzomib & ATG7 inhibitor (1 μM & 25 μM, respectively; 1h pretreatment) and cycloheximide (25 μg/ml; 2h pretreatment) for 4h following acid stripping. n=3 for vehicle, ATG7 inhibitor, and carfilzomib treatments. For both experiments, limma test was performed for significance. Only antigens significantly increased by carfilzomib are depicted. Scatterplots depict the log2 fold change of antigens for the following comparisons: carfilzomib versus vehicle (x-axis) and carfilzomib & leupeptin versus vehicle (y-axis), as well as carfilzomib versus vehicle (x-axis) and carfilzomib & ATG7 inhibitor versus vehicle (y-axis). Simplified localization of antigen source proteins is color coded. **(G)** HCC38BL cells were treated with carfilzomib (1 μM; 1h pretreatment), competition peptides known to bind HLA-A*03:01 and HLA-B*35:03 (20 ug/ml TIAPALVSK and YPTTTISYL, respectively; 1h pretreatment), carfilzomib & competition peptides (1 μM & (20 ug/ml each, respectively; 1h pretreatment) and cycloheximide (25 μg/ml; 2h pretreatment) for 4h following acid stripping. n=3 for vehicle, competition peptides, and carfilzomib treatments. Limma test was performed for significance. Scatterplot depicts the log2 fold change of antigens for the following comparisons: carfilzomib versus vehicle (x-axis) and carfilzomib & competition peptides versus vehicle (y-axis). Antigens significantly different between carfilzomib and carfilzomib + competition peptide treatments are depicted in black. **(H)** Enrichment of proteins interacting with source proteins for antigens significantly increased versus antigens significantly decreased in cells treated with MLN7243 or carfilzomib. Cells were treated as in Figure 2B. Protein interactors of source proteins for antigens significantly increased and antigens significantly decreased by MLN7243 and carfilzomib were obtained from BioGRID. The Cochran–Mantel–Haenszel test was used to test the enrichment of protein interactions across all cell lines. Bonferroni corrected adjusted p-values are indicated for significantly enriched interactors. “#” indicates insufficient interactions to calculate significance. ”-Inf” reflects no interactions in the increased antigen group.

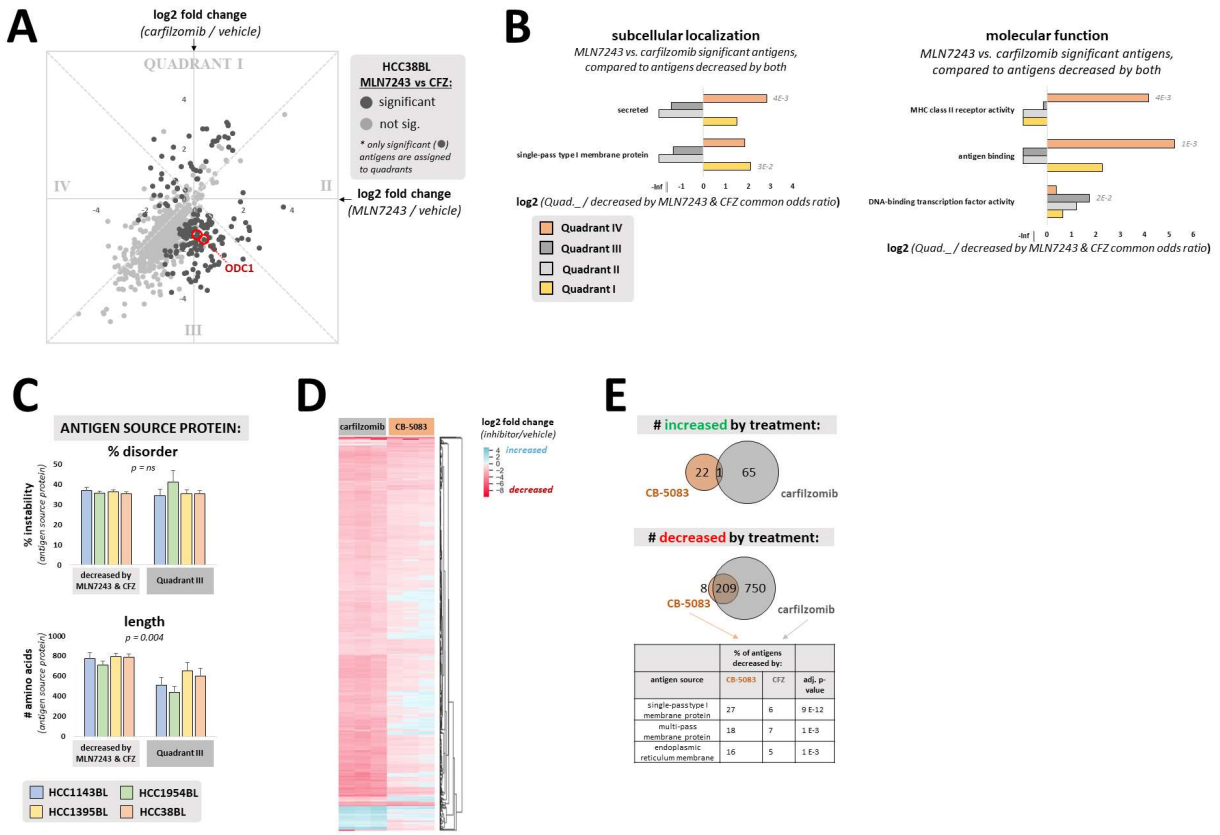

Figure 3. Antigens only partially dependent on the ubiquitin-proteasome system share unifying characteristics. (A) HCC38BL cells were treated with MLN7243 (500 nM; 4h pretreatment), carfilzomib (1 μM; 1h pretreatment), or cycloheximide (25 μg/ml; 2h pretreatment) for 4h following acid stripping. Limma test was performed for significance, and antigens not decreasing more than 1.5 fold in response to cycloheximide (n=2) in both replicates were subsequently excluded. n=3 for vehicle, MLN7243, and carfilzomib treatments. Scatterplot depicts the log2 fold change of antigens for the following comparisons: MLN7243 versus vehicle (x-axis), and carfilzomib versus vehicle (y-axis). Antigens significantly different between MLN7243 and carfilzomib treatment are indicated in darker gray. Dashed perpendicular lines delineate "quadrants"; antigens from the reported proteasome-dependent, ubiquitin-independent substrate ODC1 are marked. **(B)** HCC1143BL, HCC1954BL, HCC1395BL, and HCC38BL cells were treated as in Figure 3A. Antigens significantly different between MLN7243 and carfilzomib treatment were assigned to quadrants as in Figure 3A; antigens in each quadrant were compared to antigens significantly decreased by both MLN7243 and carfilzomib (CFZ). Subcellular localization and molecular function for antigens in these groups were obtained from UniProt. The Cochran–Mantel–Haenszel test was used to test the enrichment of terms across all cell lines. Bonferroni corrected adjusted p-values are indicated for significantly enriched terms. **(C)** HCC1143BL, HCC1954BL, HCC1395BL, and HCC38BL cells were treated as in Figure 3A. Proteins assigned to QIII (significantly decreased more by carfilzomib versus MLN7243 treatment) were compared with proteins significantly decreased by both MLN7243 and carfilzomib treatment. The percent disorder and length of each source protein was calculated; significance was determined by Fisher's method combining significance by t-test across all cell lines. ns, non-significant. **(D)** HCC1954BL cells were treated with carfilzomib (1 μM; 1h pretreatment), p97 inhibitor CB-5083 (5 μM; 1h pretreatment), or cycloheximide (25 μg/ml; 2h pretreatment) for 4h following acid stripping. Limma test was performed for significance, and antigens

not decreasing more than 1.5 fold in response to cycloheximide (n=2) in both replicates were subsequently excluded. n=3 for vehicle, carfilzomib, and CB-5083 treatments. Heat map shows log2 fold change (CB-5083/vehicle versus carfilzomib/vehicle; red = decreased, blue = increased), and only includes antigens significant in at least one treatment. **(E)** HCC1954BL cells were treated as in Figure 3D. Venn diagrams depict the overlap of antigens significantly increased or decreased by CB-5083 and carfilzomib treatments. Subcellular localization for antigens significantly decreased by CB-5083, and antigens significantly decreased by carfilzomib, was obtained from UniProt. Significance of term enrichment (antigens decreased by CB-5083 versus antigens decreased by carfilzomib) was determined by Fisher's exact test, with Bonferroni multiple testing corrections applied to yield an adjusted (adj.) p-value.

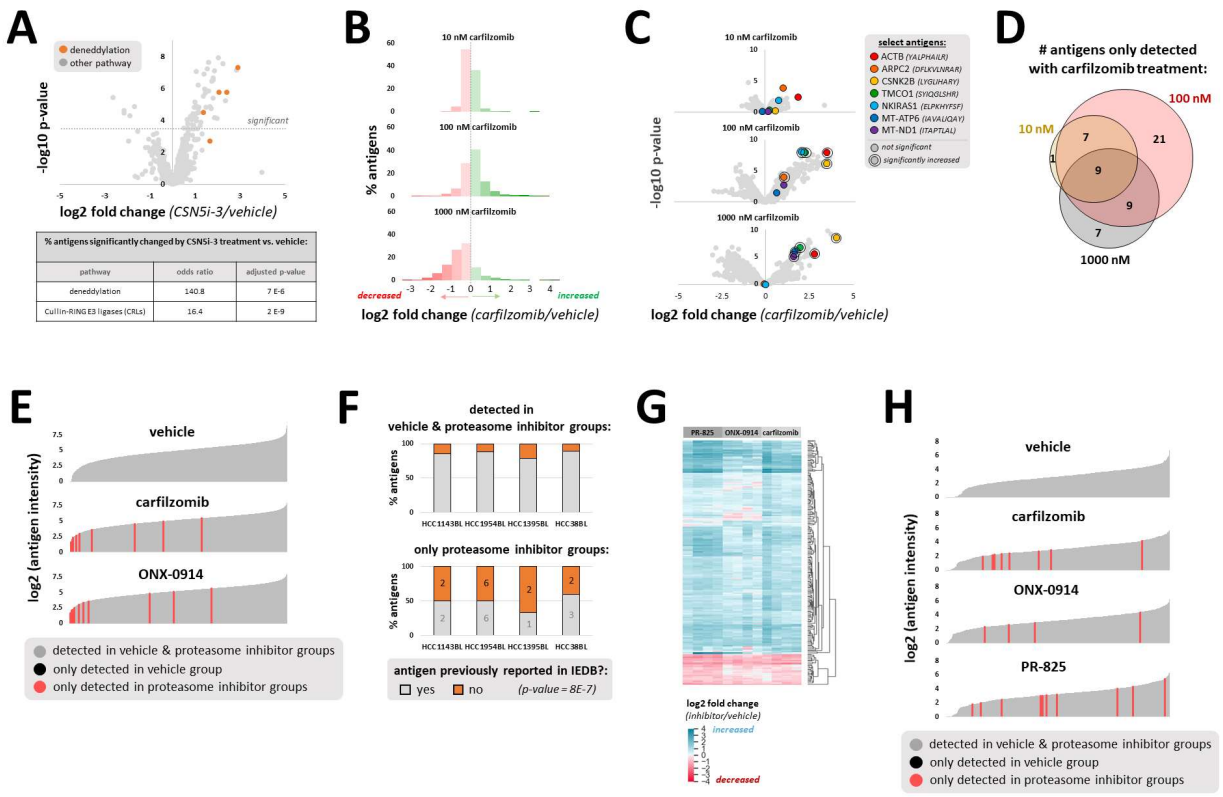

Figure 4. Atypical antigen presentation can be elicited by incomplete proteasome inhibition. (A) HCC1954BL cells were treated with MLN4924 (250 nM; 2h pretreatment), CSN5i-3 (1 µM; 2h pretreatment), or cycloheximide (25 µg/ml; 2h pretreatment) for 4h following acid stripping. Limma test was performed for significance, and antigens not decreasing more than 1.5 fold in response to cycloheximide (n=2) in both replicates were subsequently excluded. n=3 for vehicle, MLN4924, and CSN5i-3 treatments. Volcano plot represents quantitative changes in MHC Class I antigens upon CSN5i-3 treatment versus vehicle treatment. Antigen source proteins involved in deneddylation are indicated in orange. Antigen source proteins related to deneddylation and Cullin-RING E3 ligases (CRLs) were obtained from UniProt. Enrichment of these terms in antigens significantly changed by CSN5i-3 versus those not significantly changed was determined by Fisher's exact test with Bonferroni correction. **(B)** HCC1954BL cells were treated with vehicle or increasing doses of carfilzomib (1, 10, 100, & 1000 nM; 1h pretreatment) for 4h following acid stripping (n=3/treatment). Log2 fold change (carfilzomib versus vehicle; green indicates increased, red indicates decreased) is presented as histograms for 10, 100, & 1000 nM carfilzomib treatments. **(C)** HCC1954BL cells were treated as in Figure 4B. Volcano plots of the -log10(adjusted p-value), as determined by limma test, are shown. Select antigens are marked in color across 10, 100, & 1000 nM carfilzomib treatments. **(D)** HCC1954BL cells were treated as in Figure 4B. Antigens not detected in vehicle treated cells (all 3 replicates) but detected in carfilzomib treated cells (all 3 replicates at each concentration) are graphed. **(E)** HCC1954BL cells were treated with vehicle (n=3), carfilzomib (5 nM, n=4), or immunoproteasome inhibitor ONX-0914 (25 nM, n=4) for 48h to inhibit the chymotrypsin-like site of the proteasome. MHC Class I antigens were purified and quantified by mass spectrometry. Waterfall plots depict the log2 intensity of nonnormalized antigens detected in vehicle, carfilzomib, and ONX-0914 treated cells. Antigens not detected in vehicle treated cells (all 3 replicates) but detected in proteasome inhibitor treated cells (all 4 replicates) are marked in red. No antigens were detected in vehicle treated cells (all replicates) but not detected in either proteasome inhibitor treated cells (all replicates). **(F)** HCC1143BL, HCC1954BL, HCC1395BL, and HCC38BL cells were treated as

described in Figure 4C. Plots show antigens detected in both vehicle and proteasome inhibitor treated cells (all replicates; top plot), and antigens detected only in proteasome inhibitor treated cells (all replicates of carfilzomib and ONX-0914 treatment; bottom plot). Antigens bound to MHC Class I (HLA-A & HLA-B) previously reported in the Immune Epitope Database (IEDB) are shown in gray; those not previously reported are shown in orange. A Cochran–Mantel–Haenszel test was used to determine whether antigens only detected in proteasome inhibitor treated cells were more likely not to have been previously reported in IEDB; the resultant p-value is reported in the figure legend. Numbers on bottom graph represent number of antigens. **(G)** HCC1954 breast cancer cells were treated with vehicle, carfilzomib (75 nM), ONX-0914 (200 nM), or PR-825 (250 nM) for 48h. Heat map shows log2 fold change (inhibitor/vehicle), and only includes antigens significant in at least one treatment. n=4/treatment. **(H)** HCC1954 cells were treated as in Figure 4G. Waterfall plots depict the log2 intensity of nonnormalized antigens detected in vehicle, carfilzomib, ONX-0914, and PR-825 treated cells. Antigens not detected in vehicle treated cells (all 4 replicates) but detected in proteasome inhibitor treated cells (all 4 replicates) are marked in red. No antigens were detected in vehicle treated cells (all replicates) but not detected in either proteasome inhibitor treated cells (all replicates).

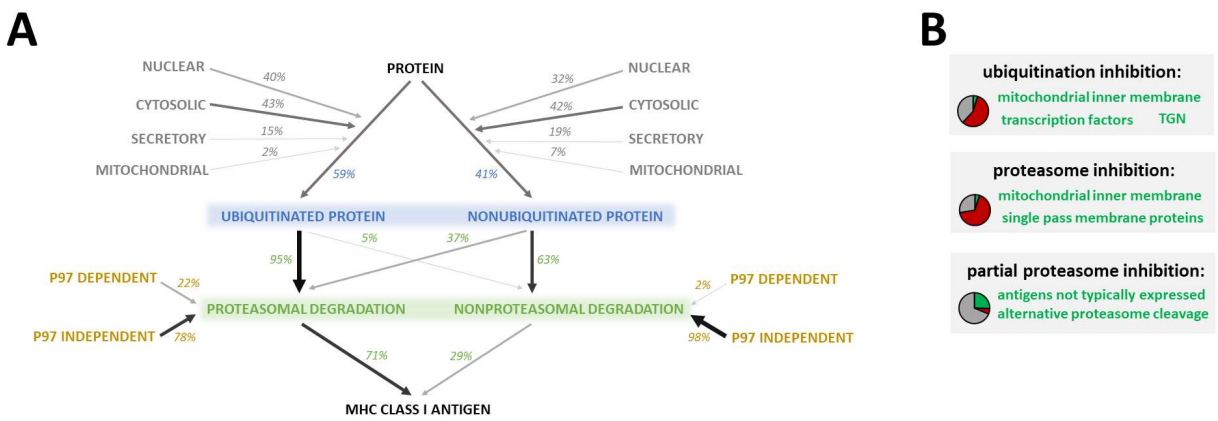

Figure 5. Diverse constitutive and compensatory protein degradation pathways produce MHC Class I antigens. (A) Quantitative summary of constitutive protein degradation pathways generating MHC Class I antigens. Numbers represent percent of antigens found to be significantly decreased in presentation by inhibition of indicated protein degradation pathways. **(B)** Summary of impact of protein degradation pathway inhibition on antigen generation. Pie charts represent relative numbers of increased (green), decreased (red), and not significantly changed (gray) antigens. Notable characteristics of significantly increased antigens (green) are provided as text.

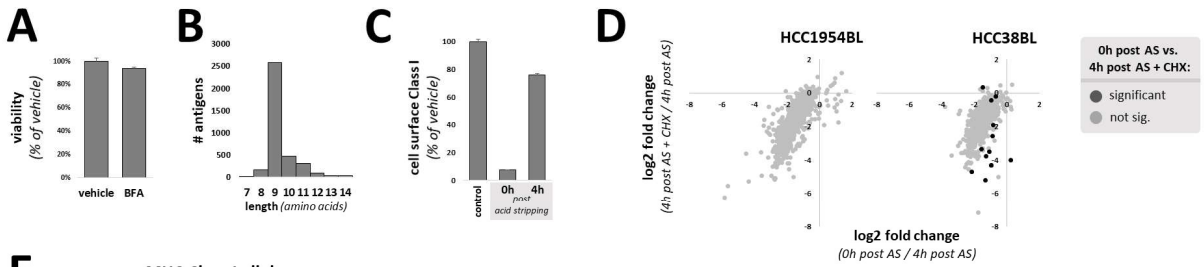

E **MHC Class I alleles:**

	HLA-A	*HLA-B*	*HLA-C*
HCC1143BL	*31:01 / 31:01*	*35:08 / 37:01*	*04:01 / 06:02*
HCC1954BL	*24:02 / 24:02*	*35:01 / 40:06*	*04:01 / 15:02*
HCC1395BL	*29:02 / 29:02*	*08:01 / 45:01*	*06:02 / 07:01*
HCC38BL	*03:01 / 03:01*	*35:03 / 35:03*	*12:03 / 12:03*

Supplemental Figure 1, related to Figure 1. (A) Viability of HCC1954BL cells treated with 5 µM Brefeldin A (BFA) for 16h, as measured by trypan blue staining, relative to viability of vehicle treated cells. Graph represents average + SEM, n=5/group. **(B)** Histogram of antigen length (# amino acids) for HCC1954BL cells treated with vehicle or Brefeldin A for 16. **(C)** Flow cytometry measurement of cell surface MHC Class I (W6/32 antibody) for untreated HCC1954BL cells (control), those collected immediately following mild acid elution to remove MHC Class I antigens (0h post acid stripping), and those collected 4h after acid stripping (n=3/group). Graph represents average + SEM. **(D)** Cells were pre-treated with vehicle, cycloheximide (25µg/ml), or Brefeldin A (5 µM) for 2h, and pre-existing antigens removed by mild acid elution ("acid stripping"; AS). Cells were immediately collected after AS, or treated again with vehicle, cycloheximide, or BFA for 4h. Significance of treatment effect was determined by limma test. Scatterplots show the log2 fold change in displayed antigens from cells collected immediately after AS versus those collected 4h after AS (x-axis) or from cells collected 4h after AS with cycloheximide treatment versus those collected 4h after AS (y-axis). Darker gray indicates antigens significantly different between cells collected immediately after AS versus those collected 4h after AS with cycloheximide treatment. **(E)** MHC Class I alleles for *HLA-A*, *-B*, & *-C* genes for B lymphoblast cell lines used *(Boegel, Castle, et al., 2014).*

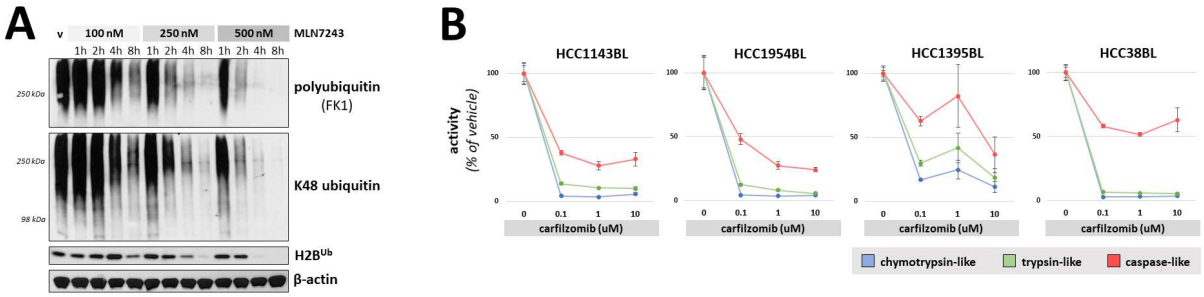

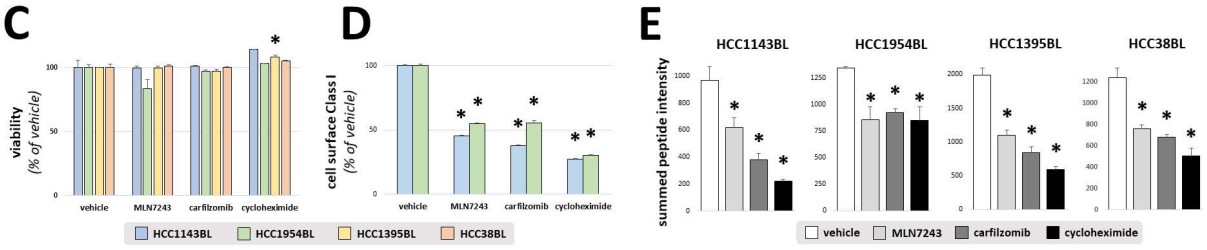

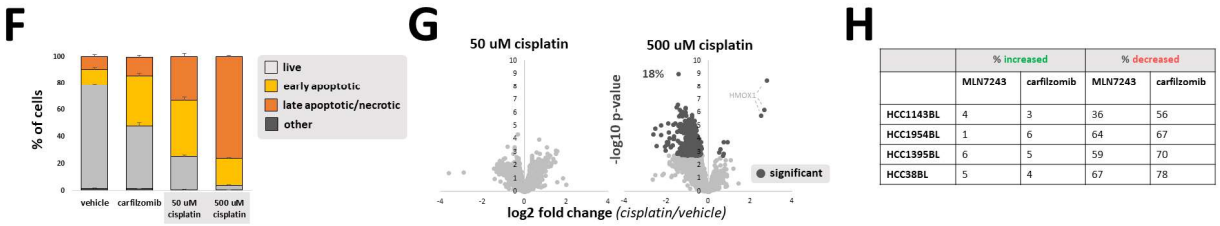

H

	% increased		% decreased	
	MLN7243	carfilzomib	MLN7243	carfilzomib
HCC1143BL	4	3	36	56
HCC1954BL	1	6	64	67
HCC1395BL	6	5	59	70
HCC38BL	5	4	67	78

I

antigens increased in 2+ cell lines:

MLN7243	carfilzomib:
AKIRIN2	C9JAW5
C9JAW5	CAT
CCT8	H2AC20
EIF4G1	LONP2
GGA2	MT-CO2
HDLBP	PHB
MT-ND6	PLIN2
NRBP1	TMSB10
ODC1	
PHB	
RRM2	
STK17A	
TMSB10	
TSEN34	

*increased in 1+ cell line by MLN7243 **and** carfilzomib*

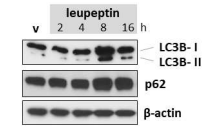

K

	% increased	% decreased
leupeptin	0	16
carfilzomib	<1	32
carfilzomib + leupeptin	<1	58

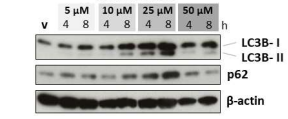

M

	% increased	% decreased
ATG7i	0	2
carfilzomib	<1	84
carfilzomib + ATG7i	<1	78

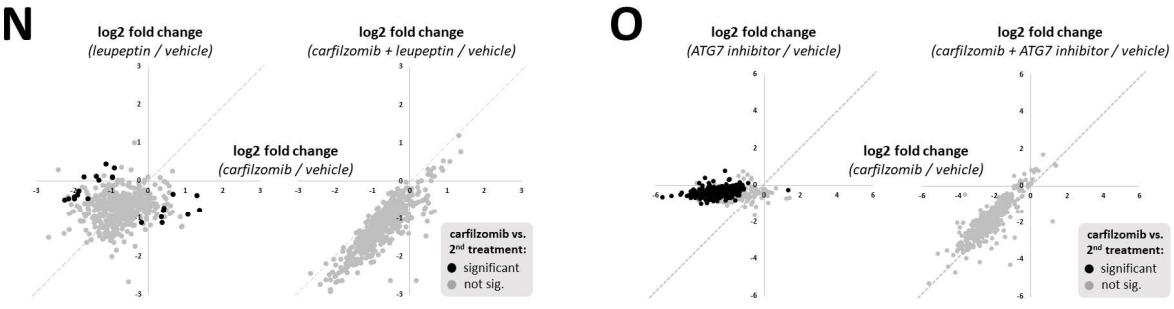

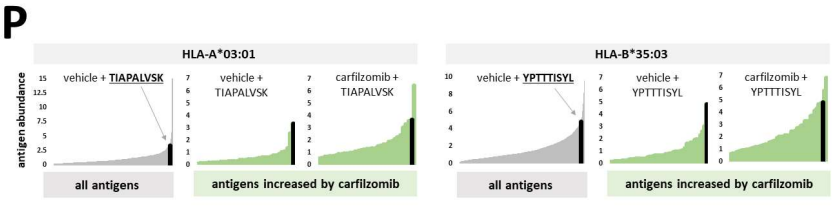

Q

predicted affinity percentile:

A*03:01 TIAPALVSK	all	75
	increased by CFZ	77
B*35:03 YPTTTISYL	all	84
	increased by CFZ	92

R

	% increased	% decreased
peptides	0	0
carfilzomib	5	20
carfilzomib + peptides	4	24

Supplemental Figure 2, related to Figure 2. (A) HCC1954BL cells were treated with doses of the E1 ubiquitination inhibitor MLN7243 as indicated, for increasing lengths of time. Polyubiquitin, K48-linked ubiquitin, and ubiquitinated histone H2B (Lys120) were immunoblotted, with β-actin used as a loading control. v, treated with vehicle. **(B)** B lymphoblast cell lines were treated with doses of the proteasome inhibitor carfilzomib as indicated for 1h. Activity of the chymotrypsin-like, trypsin-like, and caspase-like sites of the proteasome was measured using fluorescent substrates (Suc-LLVY-AMC, Boc-LRR-AMC, and Ac-nLPnLD-AMC, respectively) incubated with cell lysates for 1h at 37°C. Percent inhibition was calculated relative to vehicle treated cells (n=3/group). Graph represents average + SEM. **(C)** Viability of cells collected for mass spectrometry as measured by trypan blue staining, relative to viability of vehicle treated cells, for cells treated with MLN7243 (500 nM; 4h pretreatment), carfilzomib (1 μM; 1h pretreatment), and cycloheximide (25 μg/ml; 2h pretreatment) for 4h following acid stripping. Graph represents average + SEM (n=3 for all groups except CHX treatment, where n=2). * indicates $p < 0.01$ versus vehicle by Dunnett's test. **(D)** Flow cytometry measurement of cell surface MHC Class I (W6/32 antibody) for HCC1954BL cells treated with MLN7243 (500 nM; 4h pretreatment), carfilzomib (1 μM; 1h pretreatment), and cycloheximide (25 μg/ml; 2h pretreatment) for 4h following acid stripping. Graph represents average + SEM (n=3/group). * indicates $p < 0.01$ versus vehicle by Dunnett's test. **(E)** Summed peptide intensity quantified by mass spectrometry for cells treated with MLN7243 (500 nM; 4h pretreatment), carfilzomib (1 μM; 1h pretreatment), or cycloheximide (25 μg/ml; 2h pretreatment) for 4h following acid stripping. Graph represents average + SEM (n=3 for all groups except CHX treatment, where n=2). * indicates $p < 0.01$ versus vehicle by Dunnett's test. **(F)** Percent of HCC1954BL cells considered early apoptotic, late apoptotic/necrotic, live (not apoptotic or necrotic), or unclassifiable ("other") after the following treatments for 4h post acid stripping: vehicle, 1 μM carfilzomib (1h pre-treatment), 50 μM cisplatin (20h pre-treatment), or 500 μM cisplatin (20h pre-treatment). Staining for Annexin V was considered indicative of apoptosis, and staining for propidium iodide indicative of necrosis. Graph represents average + SEM (n=3/group). **(G)** Volcano plots representing quantitative changes in MHC Class I antigens upon cisplatin treatment (dark gray indicates significant by limma test). Cells were treated for 4h post acid stripping with the following treatments: vehicle (n=3), 50 μM cisplatin (20h pre-treatment; n=4), and 500 μM cisplatin (20h pre-treatment; n=4). **(H)** Percent antigens significantly increased or decreased by MLN7243 or carfilzomib treatment. Cells were treated with MLN7243 (500 nM; 4h pretreatment), carfilzomib (1 μM; 1h pretreatment), or cycloheximide (25 μg/ml; 2h pretreatment) for 4h following acid stripping. Limma test was performed for significance, and antigens not decreasing more than 1.5 fold in response to cycloheximide (n=2) in both replicates were subsequently excluded. n=3 for vehicle, MLN7243, and carfilzomib treatments in each cell line. **(I)** Cells were treated as described in Supplemental Figure 1H. Antigens significantly increased by MLN7243 or carfilzomib treatment in at least 2 of 4 cells lines are listed. Yellow indicates the antigen was significantly increased by MLN7243 and carfilzomib in at least 1 of 4 cell lines. **(J)** HCC1954BL cells were treated with 50 μM leupeptin for timepoints indicated, and lysates were immunoblotted for LC3B, p62, and loading control β-actin. **(K)** HCC1954BL cells were treated with carfilzomib (1 μM; 1h pretreatment), leupeptin (50 μM; 1h pretreatment), carfilzomib & leupeptin (1 μM & 50 μM, respectively; 1h pretreatment) and cycloheximide (25 μg/ml; 2h pretreatment) for 4h following acid stripping. Limma test was performed for significance (inhibitor versus vehicle), and antigens not decreasing more than 1.5 fold in response to cycloheximide (n=2) in both replicates were subsequently excluded. n=3 for vehicle, carfilzomib, and leupeptin treatments. Chart indicates percent of antigens significantly increased or decreased by each treatment. **(L)** HCC1954BL cells were treated with 5, 10, and 25 μM ATG7 inhibitor for timepoints indicated, and lysates were immunoblotted for LC3B, p62, and loading control β-actin. **(M)** HCC1954BL cells were treated with carfilzomib (1 μM; 1h pretreatment), ATG7 inhibitor (25 μM; 1h pretreatment), carfilzomib & ATG7 inhibitor (1 μM & 25 μM, respectively; 1h pretreatment) and cycloheximide (25 μg/ml; 2h pretreatment) for 4h following acid stripping. Limma test was performed for significance

(inhibitor versus vehicle), and antigens not decreasing more than 1.5 fold in response to cycloheximide (n=2) in both replicates were subsequently excluded. n=3 for vehicle, carfilzomib, and ATG7 inhibitor treatments. Chart indicates percent of antigens significantly increased or decreased by each treatment. **(N)** Cells were treated as described in Supplemental Figure 2K. Scatterplots depict the log2 fold change of antigens for the following comparisons. Left panel: carfilzomib versus vehicle (x-axis) and leupeptin versus vehicle (y-axis), and carfilzomib versus vehicle (x-axis). Right panel: carfilzomib & leupeptin versus vehicle (y-axis). Antigens significantly different between two treatments being compared are indicated in black. Dashed line depicts perfect correlation. **(O)** Cells were treated as described in Supplemental Figure 2M. Scatterplots depict the log2 fold change of antigens for the following comparisons. Left panel: carfilzomib versus vehicle (x-axis) and ATG7 inhibitor versus vehicle (y-axis). Right panel: carfilzomib versus vehicle (x-axis) and carfilzomib & ATG7 inhibitor versus vehicle (y-axis). Antigens significantly different between two treatments being compared are indicated in black. **(P)** HCC38BL cells were treated with carfilzomib (1 μM; 1h pretreatment), competition peptides known to bind HLA-A*03:01 and HLA-B*35:03 (20ug/ml TIAPALVSK and YPTTTISYL, respectively; 1h pretreatment), carfilzomib & competition peptides (1 μM & 20 ug/ml each, respectively; 1h pretreatment) or cycloheximide (25 μg/ml; 2h pretreatment) for 4h following acid stripping. n=3 for vehicle, competition peptides, and carfilzomib treatments. Limma test was performed for significance. Waterfall plots with gray bars depict the average antigen intensity for antigens after vehicle + competition peptide treatment, separated by predicted HLA allele binding. Waterfall plots with green bars depict only antigens significantly increased by carfilzomib treatment, separated by predicted HLA allele binding; the first plot depicts antigen intensity after vehicle + competition peptide treatment, and the second plot depicts antigen intensity after carfilzomib + competition peptide treatment. Black bars depict the intensity of competition peptides observed after these treatments. **(Q)** Cells were treated as described in Supplemental Figure 2P. Antigen affinity for HLA-A*03:01 and HLA-B*35:03 was predicted using NetMHCpan EL 4.1; the HLA allele with the highest predicted score was assigned to the antigen. The following groups of antigens were assessed, separated by predicted HLA allele: all antigens, and antigens significantly increased by carfilzomib treatment. The predicted affinity for the competition peptides (TIAPALVSK for HLA-A*03:01; YPTTTISYL for HLA-B*35:03) was similarly determined; chart indicates the percentile the predicted affinity of the competition peptide is in versus other peptides of the indicated group. **(R)** Cells were treated as described in Supplemental Figure 2P. Limma test was performed for significance (inhibitor versus vehicle), and antigens not decreasing more than 1.5 fold in response to cycloheximide (n=2) in both replicates were subsequently excluded. n=3 for vehicle, carfilzomib, and competition peptide treatments. Chart indicates percent of antigens significantly increased or decreased by each treatment.

A

% of significant antigens
(MLN7243 vs carfilzomib):

	QI	QII	QIII	QIV
HCC1143BL	1	2	7	0
HCC1954BL	4	0	5	5
HCC1395BL	2	2	11	1
HCC38BL	3	1	11	2

B

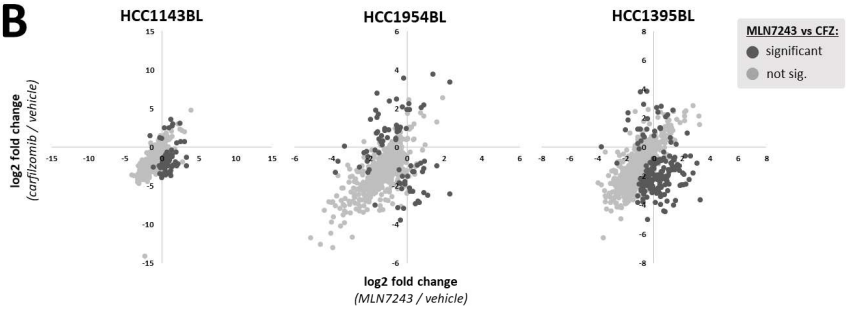

C

 # intrinsically disordered:

	QIII	UPS-dependent
HCC1143BL	2/39	8/177
HCC1954BL	1/25	18/294
HCC1395BL	9/113	28/538
HCC38BL	11/111	31/581

(p-value = 0.09)

Supplemental Figure 3, related to Figure 3. (A) HCC1143BL, HCC1954BL, HCC1395BL, and HCC38BL cells were treated with MLN7243 (500 nM; 4h pretreatment), carfilzomib (1 µM; 1h pretreatment), or cycloheximide (25 µg/ml; 2h pretreatment) for 4h following acid stripping. Limma test was performed for significance, and antigens not decreasing more than 1.5 fold in response to cycloheximide (n=2) in both replicates were subsequently excluded. n=3 for vehicle, MLN7243, and carfilzomib treatments. Antigens significantly different between MLN7243 and carfilzomib treatment were assigned to "quadrants", as indicated in Figure 3A. Table displays percent of antigens in each quadrant by cell line. **(B)** Cells were treated as in Supplemental Figure 3A. Scatterplot depicts the log2 fold change of antigens for the following comparisons: MLN7243 versus vehicle (x-axis), and carfilzomib versus vehicle (y-axis). Antigens significantly different between MLN7243 and carfilzomib treatment are indicated in darker gray. **(C)** Number of proteins in QIII and "UPS-dependent" (significantly reduced by MLN7243 and CFZ) considered "intrinsically disordered" as classified by DisProt. A Cochran–Mantel–Haenszel test was used to determine whether the fraction of antigens considered intrinsically disordered across cell lines differed between the QIII and UPS-dependent groups.

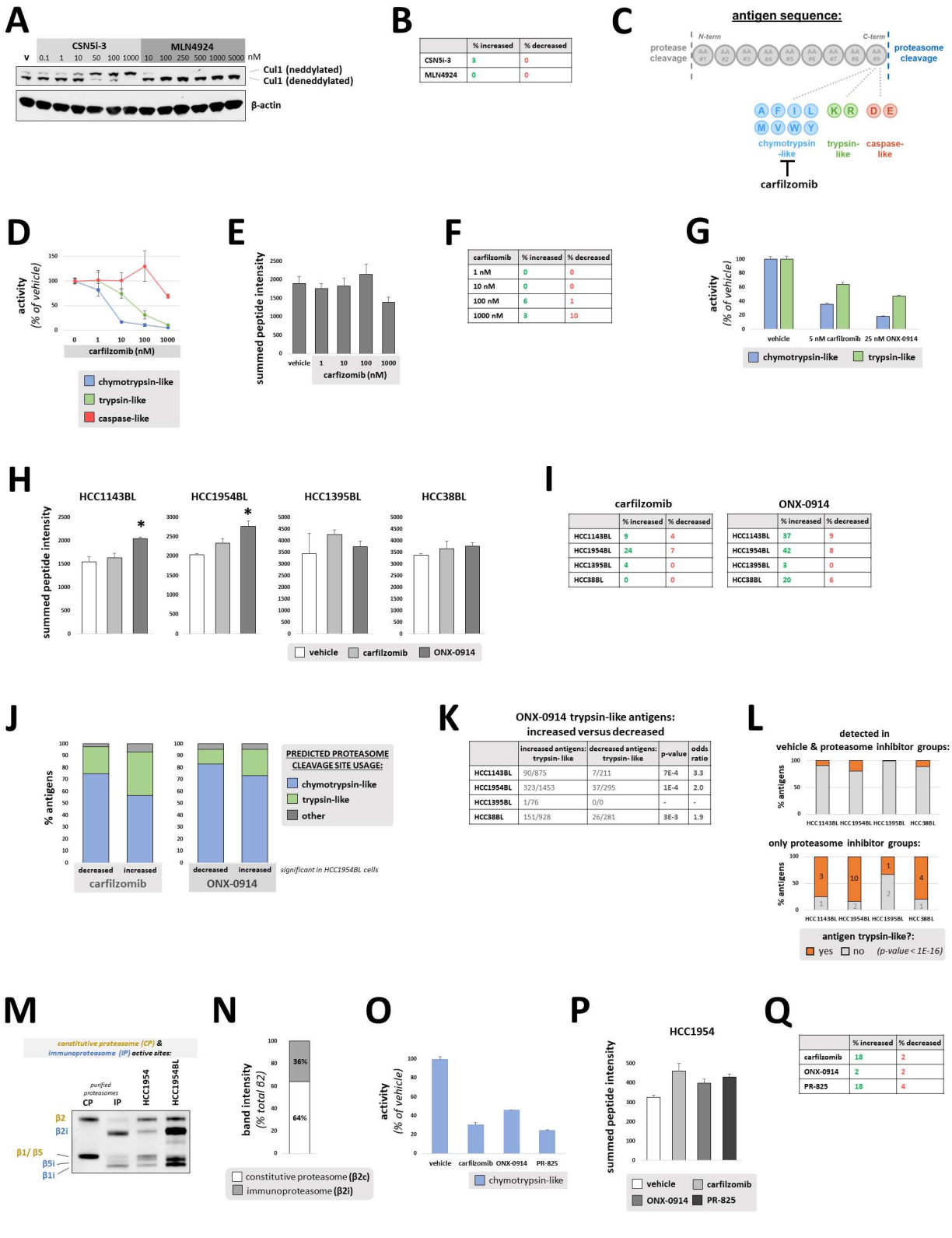

Supplemental Figure 4, related to Figure 4. (A) HCC1954BL cells were treated with increasing doses of neddylation inhibitor MLN4924 or COP9 signalosome inhibitor CSN5i-3 for 2h. Lysates were immunoblotted for neddylated/deneddylated CUL1, with β-actin used as a loading control. **(B)**

HCC1954BL cells were treated with MLN4924 (250 nM; 2h pretreatment), CSN5i-3 (1 μM; 2h pretreatment), or cycloheximide (25 μg/ml; 2h pretreatment) for 4h following acid stripping. Limma test was performed for significance, and antigens not decreasing more than 1.5 fold in response to cycloheximide (n=2) in both replicates were subsequently excluded. n=3 for vehicle, MLN4924, and CSN5i-3 treatments. Chart represents percent of antigens significantly increasing and decreasing by MLN4924 and CSN5i-3 treatment. **(C)** Graphical representation of the significance of proteasome active site usage on antigen generation. A typical 9mer antigen is depicted, with the C-terminal amino acid assumed to be generated by proteasomal cleavage. Potential C-terminal amino acids generated by the 3 types of proteasome active sites (chymotrypsin-like, trypsin-like, and caspase-like) are indicated. Carfilzomib preferentially inhibits the chymotrypsin-like site. **(D)** HCC1954BL cells were treated with vehicle (n=3) or increasing doses of carfilzomib (n=3) for 1h. Activity of the chymotrypsin-like, trypsin-like, and caspase-like sites of the proteasome was measured using fluorescent substrates (Suc-LLVY-AMC, Boc-LRR-AMC, and Z-LLE-AMC, respectively) incubated with cell lysates for 1h at 37°C. Percent inhibition was calculated relative to vehicle treated cells. Graph represents average + SEM. **(E)** HCC1954BL cells were treated with vehicle or increasing doses of carfilzomib (1, 10, 100, & 1000 nM; 1h pretreatment) for 4h following acid stripping (n=3/treatment). Graph represents average of summed peptide intensity + SEM. **(F)** HCC1954BL cells were treated as in Supplemental Figure 4E. Limma test was performed for significance. The percent of antigens that were significantly increased or decreased by each treatment is listed. **(G)** HCC1954BL cells were treated with vehicle (n=3), carfilzomib (5 nM, n=3), or immunoproteasome inhibitor ONX-0914 (25 nM, n=3) for 48h to inhibit the chymotrypsin-like site of the proteasome. Activity of the chymotrypsin-like and trypsin-like sites of the proteasome was measured using fluorescent substrates (Suc-LLVY-AMC and Boc-LRR-AMC, respectively) incubated with cell lysates for 1h at 37°C. Percent inhibition was calculated relative to vehicle treated cells. Graph represents average + SEM. **(H)** HCC1143BL, HCC1954BL, HCC1395BL, and HCC38BL cells were treated with vehicle (n=3), carfilzomib (5 nM, n=4), or immunoproteasome inhibitor ONX-0914 (25 nM, n=4) for 48h. MHC Class I antigens were purified, and limma test performed for significance (carfilzomib or ONX-0914 versus vehicle treatment). Graph depicts summed peptide intensity average + SEM (n=4 for all groups except vehicle treatment, where n=3). Significance of carfilzomib or ONX-0914 versus vehicle at $\alpha < 0.01$ by Dunnett's test is indicated by asterisks. **(I)** Cells were treated as in Supplemental Figure 4H. Tables contain percent of antigens significantly increased or decreased by carfilzomib or ONX-0914 treatment across cell lines. **(J)** HCC1954BL cells were treated as in Supplemental Figure 4H. The number of antigens considered "chymotrypsin-like (containing a C-terminal alanine, phenylalanine, isoleucine, leucine, methionine, valine, tryptophan, or tyrosine), "trypsin-like" (containing a C-terminal lysine or arginine), or "other" (all other C-terminal amino acids) was determined for antigens significantly increased and decreased by carfilzomib or ONX-0914 treatment versus vehicle. **(K)** HCC1143BL, HCC1954BL, HCC1395BL, and HCC38BL cells were treated as in Supplemental Figure 4H. The number of antigens considered "trypsin-like" (containing a C-terminal lysine or arginine) was determined for antigens significantly increased and decreased by ONX-0914 treatment versus vehicle. Significance was determined by Fisher's exact test. **(L)** HCC1143BL, HCC1954BL, HCC1395BL, and HCC38BL cells were treated as described in Supplemental Figure 4H. Plots show antigens detected in both vehicle and proteasome inhibitor treated cells (all replicates; top plot), and antigens detected only in proteasome inhibitor treated cells (all replicates of carfilzomib and ONX-0914 treatment; bottom plot). "Trypsin-like" antigens (containing a C-terminal lysine or arginine) are shown in orange; all other antigens are shown in gray. A Cochran–Mantel–Haenszel test was used to determine whether antigens only detected in proteasome inhibitor treated cells were more likely to be "trypsin-like"; this p-value is reported in the figure legend. Numbers on bottom graph represent number of antigens. **(M)** HCC1954 and HCC1954BL cells were treated with 500 nM Me4BodipyFL-Ahx3Leu3VS for 1h to label proteasome active sites. Cells were lysed and equivalent protein amounts loaded onto Tricine SDS-PAGE gels to resolve constitutive

proteasome (yellow) and immunoproteasome (blue) subunits. Purified constitutive proteasome (CP) and immunoproteasome (IP) were analyzed in parallel as a control. **(N)** Quantification of trypsin-like proteasome active site fluorescent gel band intensities as a measure of immunoproteasome to constitutive proteasome ratios in HCC1954 cells. Intensities of β2 (constitutive proteasome trypsin-like site) and β2i (immunoproteasome trypsin-like site) bands were calculated from the gel in Supplemental Figure 4M using ImageJ. Intensity ratios are depicted. **(O)** HCC1954 cells were treated with vehicle, 75 nM carfilzomib, 200 nM immunoproteasome inhibitor ONX-0914, or 250 nM constitutive proteasome inhibitor PR-825 for 48h. Activity of the chymotrypsin-like site of the proteasome was measured using a fluorescent substrate (Suc-LLVY-AMC) incubated with cell lysates for 1h at 37°C. Percent inhibition was calculated relative to vehicle treated cells (n=3/group). Graph represents average + SE. **(P)** HCC1954 breast cancer cells were treated with vehicle, carfilzomib (75 nM), ONX-0914 (200 nM), or PR-825 (250 nM) for 48h. Limma test was used to calculate significance (inhibitor versus vehicle; n=4/treatment). Graph depicts summed peptide intensity average + SEM. **(Q)** HCC1954 cells were treated as in Supplemental Figure 4P. Percent antigens significantly increased or decreased by each treatment is listed in chart.